ACS APPLIED NANO MATERIALS

www.acsanm.org Article

Cold Atmospheric Plasma-Assisted Deposition of SiO_x Nanocoatings to Enhance Stability of Pharmaceutical Tablets

Advika Vidhyadhiraja, Akshay Krishnakumar, Devendra Sarnaik, Zhongxia Shang, Kinam Park, and Rahim Rahimi*

Cite This: *ACS Appl. Nano Mater.* 2026, 9, 8294–8310 Read Online

ACCESS | Metrics & More | Article Recommendations | Supporting Information

ABSTRACT: Oral pharmaceutical formulations require long-term physicochemical stability to preserve therapeutic efficacy and maintain consistent drug quality across diverse storage and distribution environments. However, maintaining the performance of moisture-sensitive formulations in harsh and variable environments remains a persistent challenge. Recent advances in nanocoating technologies have generated significant interest as next-generation strategies to improve the stability and long-term shelf life of oral pharmaceutical formulations, yet challenges in coating efficiency, scalability, and conformal deposition on complex tablet geometries remain. Here, we report a scalable cold atmospheric plasma (CAP)-assisted approach for the direct and conformal deposition of silicon oxide (SiO_x) thin-film nanocoatings to enhance moisture barrier performance and extend tablet shelf life, using amoxicillin tablets as a model formulation. A systematic optimization of plasma scan speed and nozzle-to-substrate distance enabled uniform SiO_x deposition while minimizing thermal exposure to the tablet. The optimized SiO_x nanocoating was comprehensively characterized to evaluate the long-term moisture barrier performance and stability under accelerated aging conditions. Compared with pristine tablets, SiO_x-nanocoated tablets exhibited significantly enhanced stability, retaining over 50% of their initial chemical structure, crystallinity, and antibiotic content for up to 16 days under elevated temperature and humidity (75% RH, 40 °C). Furthermore, the coated tablets maintained broad-spectrum antibacterial activity against *Staphylococcus aureus* and *Escherichia coli* for 8 days, extending functional performance by 6 days relative to pristine controls while preserving cytocompatibility throughout the exposure period. Overall, this work demonstrates a scalable, conformal, and low-thermal-load plasma nanocoating strategy that substantially enhances the stability and shelf life of moisture-sensitive pharmaceutical tablets, offering a promising alternative for reliable drug protection in demanding storage and distribution environments.

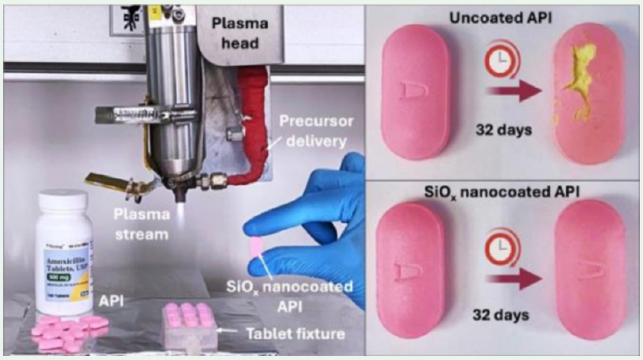

KEYWORDS: *SiO_x functional nanocoating, cold atmospheric plasma, enhanced pharmaceutical stability, amoxicillin, antibiotic stability*

1. INTRODUCTION

Pharmaceutical formulations define the engineered interface between drug discovery and clinical application, enabling the transition of active pharmaceutical ingredients (API) into stable, effective, and patient-ready therapies.[1,2] Their evolution has shaped global healthcare by enabling precise delivery, controlled release, and reliable pharmacological performance across increasingly complex and chronic disease landscapes.[1] This advancement has driven significant expansion in the pharmaceutical sector, with the U.S. market valued at $634.3 billion in 2024 and projected to grow at a compound annual rate of 5.72% through 2030, owing to the rising chronic disease burden, population aging, and broader access to healthcare.[3] Addressing these demands necessitates the development and application of diverse administration routes, including oral, inhalation, injection, transdermal, nasal, and ocular delivery systems.[4] Among these, injection, transdermal, and inhalation routes offer advantages such as rapid absorption and precise drug delivery but are often associated with limitations, including cannula-related infections, thrombophlebitis, and patient discomfort.[5] Additionally, such formulations require specialized storage systems and contribute to increased logistical complexity and resource demands, including syringes, sterilization procedures, and administration by trained personnel.[5] For example, injectable drugs such as insulin, diazepam, isoproterenol, and lorazepam have been shown to lose between

Received: February 23, 2026
Revised: April 10, 2026
Accepted: April 19, 2026
Published: April 28, 2026

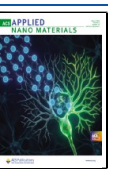

11% and 75% of their intended potency within 4 weeks to 7 months when stored at room temperature (15 to 30 °C).[6,7]

In contrast, oral solid dosage forms, particularly tablets, account for over 53% of all pharmaceutical formulations and are widely preferred due to their production efficiency, ease of administration, high patient compliance, and elimination of the need for specialized storage or handling.[8] However, despite these advantages, oral formulations remain susceptible to chemical and physical degradation pathways such as hydrolysis, oxidation, polymorphic transitions, and crystallization, often accelerated by environmental stressors including moisture, oxygen, light, heat, and mechanical stress.[9,10] Among these, environmental hydrolysis, oxidation, and thermal degradation account for nearly 87% of all reported degradation pathways across pharmaceutical samples and have been consistently identified as the dominant mechanisms affecting the stability of oral APIs, posing major challenges for maintaining efficacy under real-world storage and handling conditions.[11] During hydrolysis, water vapor absorbed from the environment into the tablet matrix cleaves labile chemical bonds such as esters, amides, and β-lactam groups, resulting in potency loss and altered pharmacokinetics.[12] Thermal degradation accelerates molecular rearrangements, promotes oxidative reactions, and induces volatilization of sensitive components at elevated temperatures, further amplifying degradation risks.[13] These processes undermine the structural integrity, disintegration properties, and dissolution performance of oral dosage forms, reinforcing the need for robust protective strategies to ensure long-term stability.

To mitigate such degradation risks, pharmaceutical products employ external protective measures with packaging acting as the primary barrier against environmental stressors. Blister packs and foil pouches are widely recognized for their high effectiveness in protecting tablets from moisture and light, achieving less than 10% loss in potency.[14] However, despite their protective performance, these formats contribute significantly to plastic and foil waste, require intricate manufacturing and sealing processes, and remain susceptible to mechanical defects.[14,15] On the other hand, bulk packaging, such as high-barrier bottles, offers improved sustainability and operational efficiency by reducing the material consumption and simplifying the dispensing process.[16] Yet, bulk formats increase the exposure of tablets to ambient air and moisture during repeated openings, heightening degradation risk over time.[17] For example, in a stability study, Khan et al. reported that packaged amoxicillin and clavulanic acid content decreased by approximately 20% within just 24 h under extremely high humidity, with 33.9% of tablets failing dissolution tests and 13.6% failing dosage standards.[18] Furthermore, regulatory analyses have linked over 25% of postmarketing quality failures to issues stemming from packaging defects or environmental infiltration during in-use conditions.[19] These limitations underscore the need for intrinsic tablet-level protection to maintain stability independent of external packaging.

In this context, there is growing interest in developing protective barrier coatings applied directly to tablet surfaces to regulate dissolution kinetics, enhance bioavailability, and stabilize the API throughout the product lifecycle.[20] Film-forming polymers such as hydroxypropyl methylcellulose (HPMC) and ethyl cellulose have been widely employed to create protective layers that shield tablets from moisture, oxygen, and gastric fluids, ensuring reliable protection and controlled drug release.[21] While these coatings are typically applied using spray techniques in pan or fluidized-bed systems, which provide an effective barrier, achieving uniform coverage on complex tablet geometries remains challenging.[22] Moreover, the use of water or organic solvents during the coating process can compromise the potency of the moisture-sensitive APIs, and the relatively thick layers required, often exceeding 150 μm, may hinder dissolution and drug absorption properties.[23] To circumvent these complications, nanoscale coating technologies have emerged as a compelling and adaptable strategy, offering ultrathin, conformal layers with precise control over thickness and composition to enhance environmental shielding without altering tablet integrity.[24] In particular, physical and chemical vapor deposition techniques such as atomic layer deposition (ALD), sputtering, and plasma enhanced chemical vapor deposition (CVD) have been investigated for their ability to deposit highly uniform, biocompatible coatings, including alumina (Al_2O_3), titanium dioxide (TiO_2), zinc oxide (ZnO), and biodegradable polymers, which collectively improve moisture resistance, inhibit crystallization, and stabilize sensitive APIs against humidity, oxidation, and thermal stress.[25−29] For example, ALD-deposited AlO_x nanocoatings have been shown to significantly enhance the stability of amorphous solid dispersions (ASDs), maintaining their integrity for up to two years, compared to uncoated ASDs, which crystallized after just 19 days.[30] Similarly, TiO_2 coatings improved the photostability of vitamin C powders stored under elevated conditions, with coated samples losing only 2% of their potency over 10 weeks, whereas uncoated powders lost 9.3%.[31] However, translation of vapor-phase nanocoating strategies to pharmaceutical manufacturing remains limited by the inherently slow and batch-wise nature of ALD and related CVD techniques, where deposition of pharmaceutically relevant coating thicknesses on the order of a few hundred nanometers typically requires tens of minutes to several hours, resulting in tablet-scale throughputs of only ∼2−4 units per minute.[32−35] The reliance on specialized vacuum infrastructure and extended processing times can therefore significantly hinder scalability, necessitating further innovations to overcome current manufacturing constraints and enable the routine industrial adoption of nanocoating strategies to advance tablet stability and performance.[36,37]

Recently, cold atmospheric plasma-assisted chemical vapor deposition (CAP) has emerged as a versatile and scalable manufacturing technique for developing functional nanocoatings on diverse substrates.[37−40] This technique uses monomeric precursors activated by an atmospheric plasma jet to produce conformal, highly cross-linked polymeric barriers under ambient conditions.[41,42] Unlike conventional vacuum-based deposition methods, CAP operates at atmospheric pressure and room temperature, eliminating the need for solvents and minimizing thermal and mechanical stress on sensitive APIs.[43] Importantly, CAP scalability is enabled through expansion of the effective treatment area, plasma head mobility, and parallelization, rather than vacuum chamber volume, allowing substantially higher areal throughput while maintaining coating uniformity across multiple tablets.[44] Additionally, the ability to form ultrathin, uniform coatings under mild conditions offers clear advantages for protecting moisture-sensitive and thermally labile compounds, positioning CAP as a promising platform for scalable tablet-level protection. Among available barrier materials, silicon oxide (SiO_x) is particularly well-suited due to its exceptionally low

https://doi.org/10.1021/acsanm.6c00822
ACS Appl. Nano Mater. 2026, 9, 8294−8310

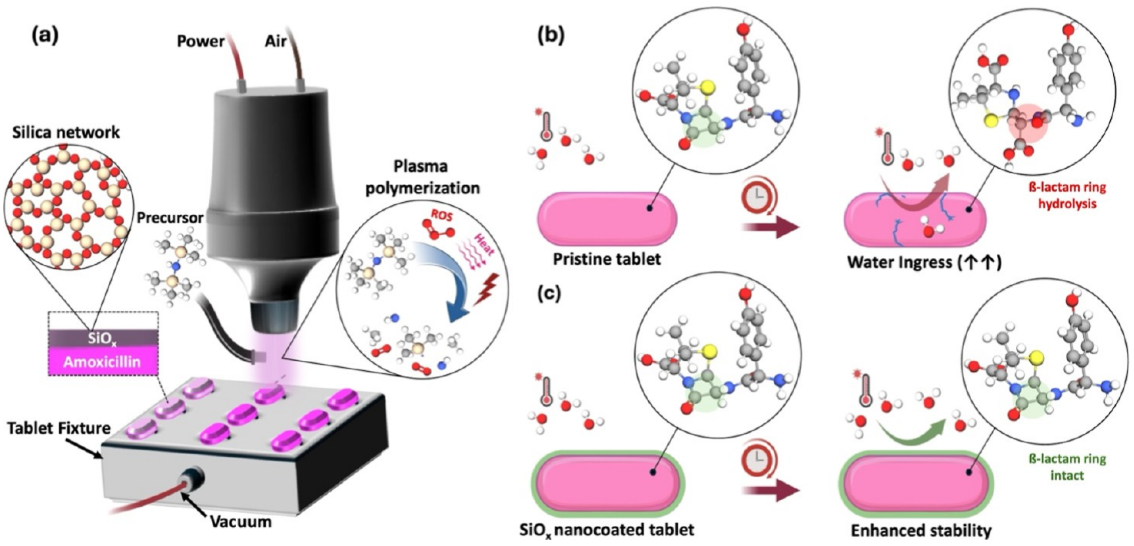

Figure 1. CAP-assisted deposition of SiO_x nanocoatings on pharmaceutical tablets for enhanced barrier protection using AMOX as a model API formulation. (a) Schematic representation of the plasma-assisted SiO_x deposition process. (b) Illustration showing hydrolytic degradation of the β-lactam ring in the pristine AMOX. (c) Enhanced barrier protection provided by the SiO_x nanocoating, with retention of the β-lactam ring upon exposure to elevated humidity conditions.

water vapor transmission rate, strong chemical inertness, and established biocompatibility.[38,39,45] In addition to its robust barrier performance, SiO_x is cost-effective and compatible with a wide range of pharmaceutical excipients, making it an attractive choice for large-scale applications. With this background, the present study demonstrates the application of CAP-assisted deposition technology to develop a SiO_x nanocoating on a model formulation containing amoxicillin trihydrate, a β-lactam antibiotic, aiming to achieve enhanced barrier protection and improved pharmaceutical stability (Figure 1a). Systematic characterization of the SiO_x nanocoating was conducted to optimize plasma-processing parameters to achieve effective moisture-barrier performance without compromising the integrity of the underlying API. The barrier performance of the optimized SiO_x nanocoating was systematically evaluated over the storage period under accelerated aging and extrapolated ambient conditions, in terms of structural integrity, functional stability, rapid release and dissolution behavior, pharmacokinetic bioavailability, antibacterial efficacy, and biocompatibility, to establish its effectiveness in preserving the quality and therapeutic performance of the nanocoated tablets, as shown in Figure 1b,c. To the best of our knowledge, this study is the first demonstration of CAP-assisted SiO_x nanocoating as a scalable, efficient, and environmentally adaptable approach for enhancing the stability and shelf life of moisture-sensitive oral dosage forms.

2. MATERIALS AND METHODS

2.1. Materials

The SiO_x precursor hexamethyldisilazane (HMDSN), employed in this study for enhanced barrier protection, was obtained from Sigma-Aldrich (MO, USA). Amoxicillin trihydrate A66 USP and penicillin potassium V 500 mg tablets (Rising Pharmaceuticals, NJ, USA), kindly provided by the Purdue College of Pharmacy (IN, USA), were used as a representative formulation to model plasma-assisted deposition of SiO_x for enhanced pharmaceutical stability. The amoxicillin trihydrate tablets contained amoxicillin trihydrate (AMOX) as the API, along with several excipients, including microcrystalline cellulose and hypromellose as fillers and binders, sodium starch glycolate and crospovidone as disintegrants, magnesium stearate as a lubricant, and Red 30 and titanium dioxide (TiO_2) in the polymeric film coating. The penicillin potassium V uncoated tablets contain penicillin as the API, along with several excipients, including anhydrous dibasic calcium phosphate, magnesium stearate, microcrystalline cellulose, and anhydrous trisodium citrate. Uncoated aspirin 325 mg tablets were obtained from HealthA2Z (NY, USA), containing aspirin as the active ingredient and corn starch as the only inactive ingredient. Tryptic soy broth (TSB), phosphate-buffered saline (PBS), agar, sodium chloride (NaCl), Mannitol salt agar (MSA), and eosin methylene blue (EMB) agar were obtained from Sigma-Aldrich (MO, USA) and used as standard media for microbial culture and enumeration. All chemicals and culture media were used as received without further modification.

2.2. Cold Atmospheric Plasma-Assisted SiO_x Nanocoating

All SiO_x nanocoatings for enhanced barrier performance against water vapor transmission were applied onto pharmaceutical tablets using a cold atmospheric-pressure plasma jet system (Plasmatreat PE39, NRW, Germany) comprising a high-frequency plasma generator and a dual-channel precursor delivery unit with independently adjustable flow rates. Compressed air was used as both the plasma-forming gas and the carrier gas for precursor delivery, enabling the generation of a stable reactive plasma plume under ambient conditions. The plasma gas was delivered to the plasma head at a flow rate of 35 $L \cdot min^{-1}$, operated at a frequency of 23 kHz and an applied voltage of 260 V, resulting in a plasma power output of 560 W. Simultaneously, the carrier gas transporting vaporized precursors into the plasma glow region was maintained at a flow rate of 10 $L \cdot min^{-1}$, while the SiO_x precursor itself was introduced at a flow rate of 10 $g \cdot h^{-1}$, ensuring stable delivery and consistent interaction within the active plasma zone. The entire plasma head assembly was mounted on a robotic platform with precision-controlled three-dimensional motion, enabling accurate control of the scan speed and nozzle-to-sample distance to ensure uniform and reproducible coating deposition across the tablet surface.

As a proof of concept, the proposed deposition technology was demonstrated using a model amoxicillin tablet containing a broad-spectrum β-lactam as the API. To immobilize the tablets within the plasma-coating region during deposition, a custom 3D-printed tablet fixture with integrated vacuum channels was fabricated via stereolithography. A fixture consisting of an array of channels, with an independent vacuum line converging to a single outlet maintained at −30 kPa to securely hold the tablets, was designed using Autodesk

https://doi.org/10.1021/acsanm.6c00822
ACS Appl. Nano Mater. 2026, 9, 8294−8310

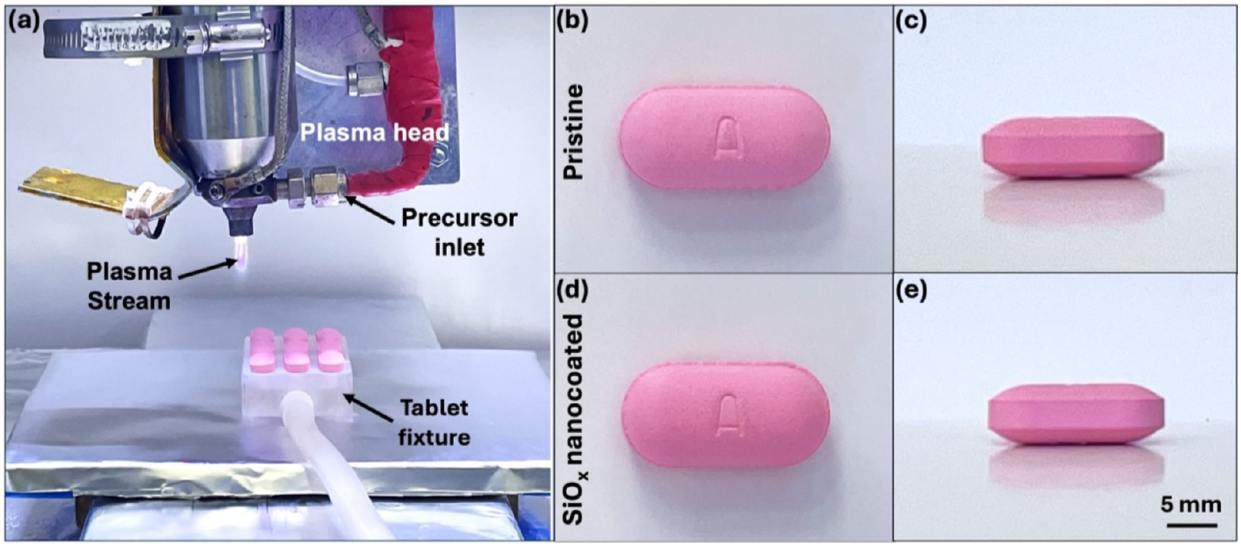

Figure 2. CAP-assisted deposition of SiO_x nanocoating on AMOX tablets. (a) Deposition setup showing the plasma head with precursor inlet directed into the plasma plume and the tablet fixture equipped with negative pressure to secure tablets during deposition. Images of the tablets including (b) top view and (c) side view of the pristine tablet, and (d) top view and (e) side view of the SiO_x-nanocoated tablets.

Inventor (CA, USA).[46] Next, the 3D-printed mold was mounted onto an $X-Y$ stage within the plasma deposition region, followed by the sterile placement of tablets in the designated slots and activation of the vacuum system. To ensure uniform coverage on either face, tablets were first coated on one face and then inverted, followed by plasma deposition on the opposite face. The complete plasma generation setup, integrated with a custom-developed 3D-printed fixture for tablet immobilization, is shown in Figure 2a.

To ensure thermal compatibility and prevent degradation of the API in the formulation during deposition, it is necessary to identify the plasma process parameters that enable efficient SiO_x deposition while preserving the tablet integrity. To achieve this, the scan speed of the plasma head was varied from 100 to 250 mm·s^{-1} in 50 mm·s^{-1} increments, and the nozzle-to-substrate distance was adjusted from 30 to 75 mm in 15 mm intervals. To achieve uniform surface coverage, the robotic system was programmed to perform two complete scans across the tablet surface with a step size of 1 mm between consecutive line passes. Substrate surface temperature was continuously monitored with a surface−contact thermocouple (NI USB TC01, National Instruments, TX, USA) to assess the extent of thermal exposure during deposition.

2.3. Surface Wettability Assessment of CAP-Nanocoated Tablets

To evaluate the effect of different plasma deposition conditions on surface wettability and potential enhancement of resistance to moisture transmission, water contact angle (WCA) measurements were performed on pristine and SiO_x-nanocoated tablets under each plasma parameter combination. The sessile drop method was used with an optical contact angle goniometer (DSA100, KRÜSS GmbH, Hamburg, Germany). A 2 μL droplet of deionized water was dispensed onto the tablet surface, and the contact angle was calculated using the Young−Laplace contour fitting method.

2.4. Morphological and Elemental Composition

To investigate the effect of plasma deposition on the tablets and distribution of SiO_x nanocoating, a series of chemical and microstructural analyses were performed. A field emission scanning electron microscope (Quanta 3D microscope, ThermoFisher, MA, USA), operated at 20 kV and 0.21 nA, and equipped with an integrated energy-dispersive X-ray spectroscopy (EDS) system operated at 15 kV, was used to examine the surface morphology and elemental composition of the tablets before and after application of SiO_x nanocoating. SEM imaging was performed at magnifications of 100× (0°), 500× (0°), 2000× (0°), and 10,000× (0°). Additionally, the functional groups and chemical bonds on the surface of SiO_x-nanocoated tablets were characterized by using attenuated total reflection Fourier transform infrared spectroscopy (ATR-FTIR). Key vibrational band spectra were acquired using a Nicolet iS5 FTIR spectrometer (Thermo Fisher Scientific, MA, USA) equipped with an iD7 diamond ATR accessory.

To directly visualize the coating morphology, cross-sectional imaging was performed using an optical microscope (Leica Biosystems, Wetzlar, Germany), with tablets sectioned along the cross plane.

2.5. Mechanical Integrity and Dissolution Assessment

To assess the mechanical stability of the SiO_x nanocoating on the tablets, the US Pharmacopeia (USP) <1216> Tablet Friability was performed. In this test, ten pristine and SiO_x-nanocoated tablets, each weighing approximately 6.5 g, were placed in a friability drum and rotated for 100 revolutions at 25 ± 1 rpm. After completion, the tablets were carefully dedusted, photographic images were obtained to assess visual changes and reweighed to determine the percentage weight loss according to pharmacopeial guidelines.[47,48]

Additionally, to evaluate the influence of the SiO_x nanocoating on tablet disintegration and drug release kinetics, dissolution testing was conducted on both pristine and SiO_x-nanocoated tablets. For this test, each tablet was placed in 1 L of phosphate buffer (pH 6.8), maintained at 37 ± 0.5 °C and agitated at 50 rpm. At predetermined time intervals (5, 10, 20, 40, and 60 min), 1 mL aliquots were withdrawn and immediately filtered through 0.22 μm syringe filters to remove particulates. The filtrates were then analyzed in triplicate using UV−visible spectroscopy (NanoDrop One^c ThermoScientific, MA, USA), with spectra acquired over a wavelength range of 190−400 nm, to assess API concentration, monitoring absorbance at wavelengths corresponding to relevant chromophores.

2.6. Accelerated Stability Assessment of SiO_x-Nanocoated Tablets

To evaluate the enhanced stability of the optimized SiO_x nanocoating and its effectiveness in limiting moisture ingress into the tablet and mitigating hydrolytic degradation of the API, an accelerated aging study was conducted under controlled stress conditions of 40 °C and 75% relative humidity (RH), in accordance with International Council for Harmonization guidelines.[9] Initially, a high-humidity chamber was established using a saturated NaCl solution placed within a sealed desiccator, which was housed in a laboratory oven maintained at 40 °C[17]. The chamber was allowed to equilibrate for 1 week prior to sample introduction to maintain stable humidity

https://doi.org/10.1021/acsanm.6c00822
ACS Appl. Nano Mater. 2026, 9, 8294−8310

conditions throughout the study. Next, the pristine and optimized SiO_x-nanocoated tablets were placed in the chamber and subjected to accelerated aging. Tablets were retrieved at predefined time points, namely, 0, 2, 4, 8, 16, and 32 days of incubation, for further characterization to evaluate the progression of physical and chemical changes over time. Photographic images of the tablets retrieved at different time points were captured to evaluate visual changes in the physical integrity of the tablets. Additionally, image-based analysis was performed using ImageJ software by quantifying the number of damaged pixels relative to the total tablet area, expressed as a percentage of surface damage. The analysis was carried out by isolating the tablet region from the background, followed by identifying surface irregularities associated with cracking, pitting, and discoloration as damaged regions. These regions were quantified relative to the total visible tablet surface to obtain a normalized measure of damage across all time points. In parallel, visual disintegration and wetting behavior were assessed by immersing each tablet in 10 mL of deionized water and capturing time-lapse images at 0, 15, and 30 s to compare disintegration screening kinetics and surface integrity.

To further investigate changes in the chemical characteristics of the pristine and optimized SiO_x-nanocoated tablets under accelerated aging, chemical stability was assessed by using attenuated total reflection Fourier transform infrared spectroscopy (ATR-FTIR). Spectra were acquired using a Nicolet iS5 FTIR spectrometer (Thermo Fisher Scientific, MA, USA) equipped with an iD7 diamond ATR accessory. Key vibrational bands of the β-lactam ring and other API-specific functional groups were monitored to detect chemical degradation from prolonged exposure to elevated temperature and humidity. Additionally, to evaluate potential changes in the crystalline structure of the API following exposure to elevated temperature and humidity, powder X-ray diffraction (XRD) analysis was performed on tablets collected at each predefined time point. Diffraction patterns were recorded using a PANalytical Empyrean diffractometer (Malvern Panalytical, Malvern, UK), equipped with a Cu Kα radiation source (λ = 1.5406 Å), operated at 45 kV and 40 mA, and fitted with a D/teX Ultra detector. For this test, samples were finely ground, mounted on stainless-steel holders, and scanned across a 2θ range of 0° to 40° to detect shifts in diffraction peaks, peak broadening, or changes in intensity indicative of recrystallization or phase transitions.[49]

2.7. Drug Concentration Analysis

To characterize the chemical species released upon dissolution of pristine and SiO_x-nanocoated tablets during the accelerated aging test, the dissolution solutions were analyzed using UV−vis spectroscopy. For this test, tablets retrieved at different aging time points were dissolved in a pH 6.8 phosphate buffer solution, maintained at 37 °C, and agitated at 75 rpm for 60 min in accordance with United States Pharmacopeia (USP) guidelines. Progressively, the resulting dissolution solutions were analyzed by acquiring UV−vis spectra from 190 to 400 nm to observe changes in absorbance, as described previously.

To qualitatively examine the individual chemical components contributing to the changes in the observed absorbance features, high-performance liquid chromatography coupled with UV−vis detection (HPLC-UV) was employed. The analysis was performed on solutions obtained from pristine and SiO_x-nanocoated tablets collected on day 8 of the accelerated aging study, with UV−vis detection at wavelengths characteristic of the API chromophores. A standard amoxicillin API, AMOX-d_4 (Cayman Chemical, MI, USA), was used as a control in this study to distinguish peaks associated with β-lactam absorption bands from those of degradation products. For this test, each tablet was individually dissolved in 1000 mL of pH 6.5 PBS buffer, agitated on a plate shaker at 75 rpm for 60 min at room temperature, and appropriately diluted for HPLC-UV. The analysis was performed on an Agilent 1200 Rapid Resolution liquid chromatography system coupled to an Agilent 6460 triple quadrupole mass spectrometer (Agilent Technologies, Santa Clara, CA, USA), using a Waters Atlantis T3 column (2.1 × 75 mm, 3.5 μm; Waters Corporation, Milford, MA, USA) for chromatographic separation. Here, the mobile phase consisted of HPLC grade water with 0.1% formic acid (v/v) as phase A and HPLC grade acetonitrile with 0.1% formic acid (v/v) as phase B, employing a linear gradient that began with 0% B for the first minute, increased linearly to 100% B between 1 and 8 min, held at 100% B from 8 to 8.5 min, then returned to 0% B at 9 min and maintained until 15 min, with a constant flow rate of 0.3 mL·min^{-1} throughout.

Furthermore, to quantify the concentration of the primary fragment (API) following accelerated aging, pristine and SiO_x-nanocoated tablets collected at each time point were analyzed by using liquid chromatography coupled with tandem mass spectrometry (LC−MS/MS). Samples were prepared and chromatographically separated using the same dissolution and HPLC conditions described above, and the resulting eluents were introduced into the mass spectrometer for analysis. The mass spectrometer was operated in the positive electrospray ionization (ESI^+) mode with multiple reaction monitoring for analyte detection, using a source gas temperature of 325 °C with a nitrogen gas flow of L·min^{-1}, a nebulizer pressure of 35 psi, and a sheath gas temperature and flow rate of 300 °C and 9 L·min^{-1}, respectively. The capillary voltage was maintained at 4000 V, along with the nozzle voltage of 1000 V, and a delta electron multiplier voltage (ΔEMV) of 400 V. Quantification of API (AMOX) was performed using an internal standard method with deuterated AMOX-d_4 spiked into each sample, and a calibration curve generated from serial dilutions of AMOX-d_4, with all data acquired and processed using Agilent Mass Hunter Quantitative Analysis software (Version 10.1).

2.8. Bactericidal Efficacy

To evaluate the bactericidal efficacy of API in pristine and SiO_x-nanocoated tablets following accelerated aging, in vitro antibacterial assays (as described in Figure S1 of the Supporting Information) were conducted using representative Gram-positive and Gram-negative bacterial strains, *Staphylococcus aureus* (ATCC 25923) and *Escherichia coli* (ATCC 25922), respectively.[46] Bacterial cultures were initially revived from frozen stocks and grown overnight in sterile TSB (30 g·L^{-1}) at 37 °C. Overnight cultures were subsequently harvested by centrifugation, washed three times with sterile PBS, and resuspended to an optical density at 600 nm ($OD_{600\ nm}$) of 0.20, corresponding to an approximate concentration of ∼10^5 CFU·mL^{-1}. Prior to the time-dependent antibacterial activity assays, the minimum inhibitory concentration (MIC) of amoxicillin in pristine and SiO_x-nanocoated tablets was determined for both *S. aureus* and *E. coli*.

A concentration gradient of amoxicillin, ranging from 0 to 10 μg·mL^{-1} in 0.5 μg·mL^{-1} increments, was prepared to identify the lowest concentration that inhibited visible bacterial growth. For the bactericidal assay, 200 μL of the diluted bacterial suspension was added to each well of a sterile 96-well plate, followed by the addition of the dissolved, appropriately diluted tablets collected at each stability time point. After 6 h of incubation at 37 °C, bacterial suspensions were serially diluted in PBS and plated onto selective and differential MSA plates for *S. aureus* and EMB plates for *E. coli*. For samples with lower bacterial concentrations, 20 μL of the API exposed bacterial suspension was plated by using the spread plate technique. The resultant plates were further incubated for 18 h at 37 °C to enumerate the colony-forming units (CFUs) and assess the residual bacterial viability. Progressively, after identifying the appropriate MIC, the change in bactericidal potency of the pristine and SiO_x-nanocoated tablets retrieved from each time-stored sample was evaluated by comparing CFU counts with the established MIC threshold, using a consistent plating and serial dilution protocol across all conditions, as described previously. All experiments were conducted in biological triplicates, with two technical replicates per condition (n = 6).

2.9. Biocompatibility Analysis

Finally, to validate the biocompatibility characteristics of the SiO_x-nanocoated tablets before and after accelerated aging, in vitro cytotoxicity assays (as described in Supporting Information Figure S2) were performed using ileocecal epithelial (HCT-8, ATCC CCL-244, VA, USA) cells. Cells between passages 8 and 10 were

https://doi.org/10.1021/acsanm.6c00822
ACS Appl. Nano Mater. 2026, 9, 8294−8310

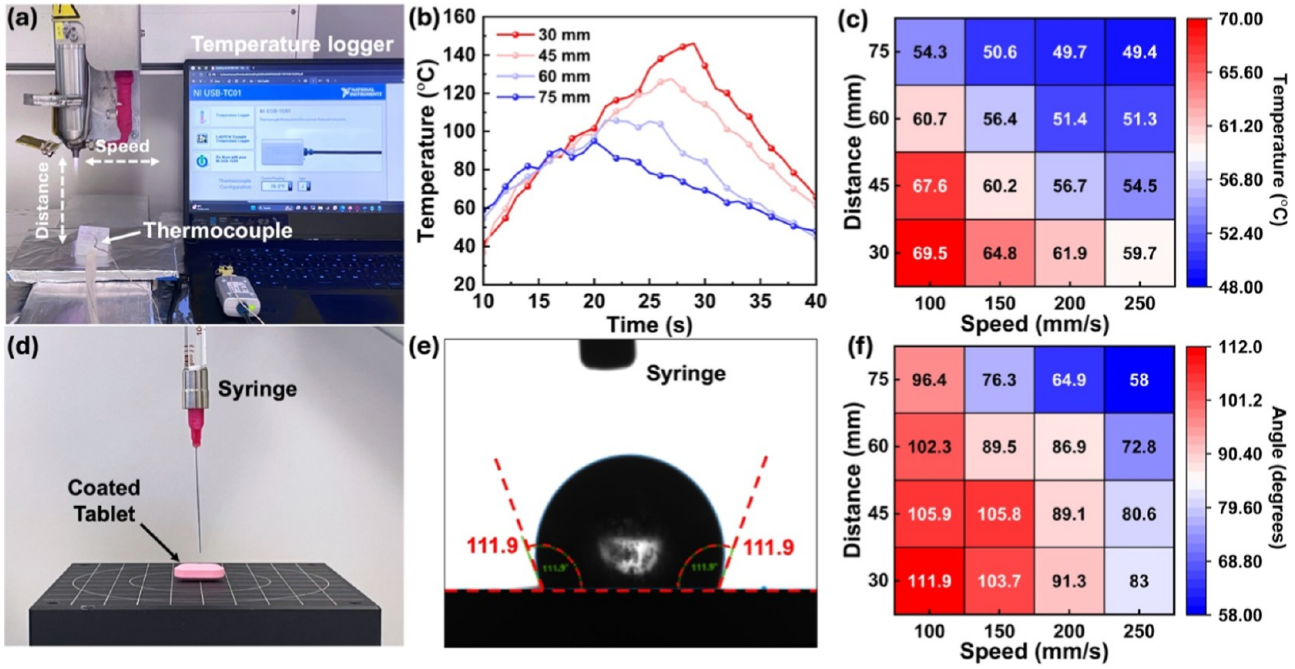

Figure 3. Optimization of the CAP-assisted SiO_x nanocoating on AMOX tablets. (a) Photographic image of the deposition process showing a thermocouple embedded within the tablet fixture to monitor surface temperature, connected to a data logger. (b) Temperature profiles recorded at different plasma heads at a fixed scanning speed of 100 mm·s^{-1} over time. (c) Heatmap depicting surface temperature variations as a function of nozzle-to-substrate distance and scanning speed. (d) Set up for surface water contact angle measurement using the sessile drop method post deposition. (e) Representative image of the water contact angle measurement on a coated tablet. (f) Heatmap depicting the surface water contact angle across various nozzle-to-substrate distances and scanning speeds.

maintained in Dulbecco's modified Eagle's medium (DMEM) supplemented with 10% fetal bovine serum (Invitrogen Inc., Carlsbad, CA). Cultures were maintained in T-75 flasks at 37 °C in a humidified incubator with 5% CO_2 until reaching approximately 80% confluence over 3 days. Cells were then detached using trypsin/EDTA (Invitrogen Inc., CA, USA), washed, resuspended in fresh medium, and diluted to a final concentration of 5000 cells·mL^{-1} for subsequent cytotoxicity evaluation. Two complementary biocompatibility assays were performed. First, the impact of the API on cellular metabolic activity was assessed via a tetrazolium salt-based MTT assay. For this, 100 μL of the diluted cell suspension was seeded into 96-well plates and allowed to adhere for 24 h before the addition of pristine and SiO_x-nanocoated tablets from each time-stored sample at a concentration of 25 μg·mL^{-1}. Following a 24 h exposure period, the materials were removed, and the MTT assay was conducted according to the manufacturer's protocol. In brief, 10 μL of MTT reagent was added to each well and incubated for 3 h, after which 200 μL of the detergent reagent was introduced. Plates were then agitated for 2 h at room temperature, and absorbance was measured at 570 nm by using a CLARIOstar microplate reader (BMG Labtech, NC, USA). To further assess changes in cell viability and morphology upon exposure of tablets from each time point, a live/dead staining assay was performed using the LIVE/DEAD Cytotoxicity Kit (ThermoFisher, MA, USA). The procedure for cell seeding and material exposure followed the same protocol as that used for the MTT assay, as described previously. After 24 h of incubation with APIs under accelerated aging conditions, samples were collected, and cells were stained with fluorescent dyes to distinguish viable from nonviable cells based on membrane integrity. Fluorescence imaging was performed using an optical Ti2 Eclipse microscope (Nikon, NY, USA) equipped with appropriate filter sets under a 10× objective, and images were processed using NIS-Elements D software.

3. RESULTS AND DISCUSSION

3.1. Deposition of SiO_x Nanocoating

Figure 2a illustrates the CAP-assisted setup used for the direct deposition of SiO_x nanocoatings onto pharmaceutical tablets. During deposition, the HMDSN precursor is exposed to high-energy electrons and reactive plasma species, leading to molecular bond fragmentation and the generation of reactive intermediate radicals.[37] These plasma-generated species subsequently undergo plasma-assisted polymerization, resulting in the formation of a highly cross-linked SiO_x network conformally deposited on the tablet surface within the plasma exposure zone.[41,42,50] Figure 2b–d shows representative images of AMOX tablets before and after CAP-assisted SiO_x nanocoating. Optical inspection indicates that both pristine and coated tablets retain the characteristic pink coloration associated with the TiO_2-based film coating, along with intact edges and well-defined "A" and "66" imprints across the curved surfaces. These observations confirm that the CAP-assisted deposition process preserves the macroscopic appearance and structural integrity of the tablets with no visible damage or deformation.

It is critical to consider that the application of functional coatings on pharmaceutical tablets is inherently constrained by the thermal sensitivity of APIs as many degrade at temperatures between 160 and 250 °C.[51,52] As such, careful optimization of the plasma deposition parameters is essential to ensure thermal compatibility with the tablets while maintaining the structural and functional integrity of the SiO_x nanocoating. To achieve this, a surface–contact thermocouple was positioned near the plasma deposition region to monitor the rise in the tablet surface temperature in real time while systematically varying the scan speed of the

https://doi.org/10.1021/acsanm.6c00822
ACS Appl. Nano Mater. 2026, 9, 8294–8310

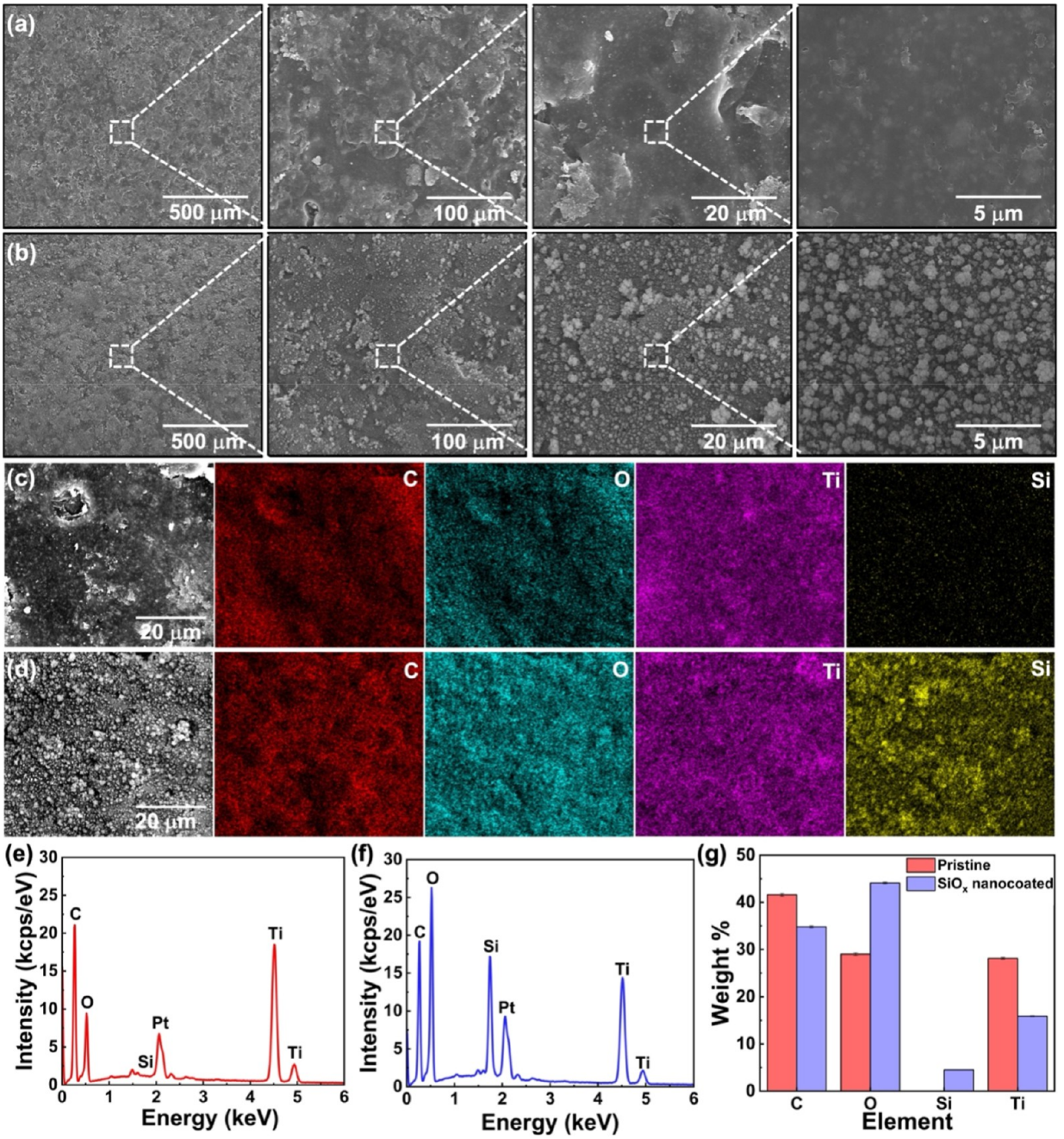

Figure 4. Morphological and elemental characterization of pristine and optimized SiO_x-nanocoated tablets. SEM images at various magnifications of (a) pristine and (b) SiO_x-nanocoated tablet surfaces. (c) Surface elemental mapping of the pristine sample and (d) SiO_x-nanocoated tablet showing the distribution of carbon, oxygen, silicon, and titanium atoms. (e) EDX spectra of the pristine surface and (f) SiO_x-nanocoated surface, with (g) the corresponding elemental composition weight percentage of C, O, Si, and Ti.

plasma jet (100 to 250 mm·s^{-1} in 50 mm·s^{-1} increments) and the nozzle-to-substrate distance (30 to 75 mm in 15 mm intervals) (Figure 3a). The surface temperature of the tablet as a function of varying plasma head heights and scan speeds is shown in Figure 3b. Overall, increasing the plasma-to-substrate distance at a constant scan speed of 100 mm·s^{-1} resulted in a clear reduction in the surface temperature. At a distance of 30 mm, the tablet surface temperature reached a peak of ∼141 °C during plasma exposure, whereas at the maximum tested distance of 75 mm, the surface peak temperature remained substantially lower at ∼92 °C (Figure 3b), indicating a significantly reduced thermal load under these conditions. To further quantify the extent of increase in baseline temperature due to plasma exposure, the average surface temperature during the coating process across all plasma deposition process combinations is visualized as a heatmap in Figure 3c. As observed, tablets treated at longer nozzle-to-substrate distances of 60 to 75 mm exhibited minimal temperature increases, with surface temperatures remaining below 60 °C across all scan speeds, for the duration of ∼20 s. On the other hand, at an intermediate distance of 45 mm, a moderate rise in temperature was recorded, ranging from 50 to 68 °C, without a substantial increase in overall surface temperature across all scanning speeds. Moreover, at the shortest distance of 30 mm,

https://doi.org/10.1021/acsanm.6c00822
ACS Appl. Nano Mater. 2026, 9, 8294−8310

although the relative change in temperature remained comparable, the absolute surface temperatures exceeded 110 °C across all scan speeds, indicating a higher thermal load that may compromise API stability.

To assess the coating's effectiveness as a moisture barrier, water contact angle measurements were performed on all SiO_x-nanocoated tablets across the plasma optimization parameters tested, as shown in Figure 3d. Initially, the pristine tablets exhibited a hydrophilic surface with a contact angle of 61.5°, which increased substantially following CAP-assisted SiO_x deposition (Supporting Information Figure S3). On the other hand, the SiO_x-nanocoated tablets processed at a lower scan speed of 100 mm·s^{-1} and a shorter nozzle-to-substrate distance of 30 mm exhibited higher hydrophobicity than those treated under faster or greater standoff conditions (Figure 3e). This behavior is attributed to the increased plasma residence time and higher effective plasma density at the tablet surface, which promote enhanced precursor fragmentation and cross-linking. These effects result in the formation of a thicker and denser SiO_x nanocoating, providing a more effective moisture barrier with improved water-repellent properties.[50] To further quantify the change in contact angle under varying plasma conditions, the measured values were visualized as a heatmap, as shown in Figure 3f. At nozzle-to-substrate distances of 60 to 75 mm, the SiO_x-nanocoated tablets did not exhibit significant hydrophobicity, with contact angles below 90° across scan speeds of 150 to 250 mm·s^{-1}. However, at the lowest scan speed of 100 mm·s^{-1}, contact angles ranged from approximately 96.4° to 102° across the higher nozzle-to-substrate distances, deviating from the otherwise hydrophilic response observed at higher nozzle-to-substrate distances. On the other hand, at an intermediate distance of 45 mm, a consistent increase in hydrophobicity was observed, with contact angles exceeding 100° at lower scan speeds and reaching up to 105.8° at 150 mm·s^{-1}. At the shortest nozzle-to-substrate distance of 30 mm, coatings exhibited high contact angles across all scan speeds. Although these processing conditions resulted in enhanced hydrophobicity, they were consistently associated with elevated surface temperatures, which may potentially limit their applicability for thermally sensitive APIs. Based on the observed trends, a nozzle-to-substrate distance of 45 mm and a scan speed of 150 mm·s^{-1} are identified as the optimized plasma processing parameters. Under these conditions, the SiO_x nanocoating achieves enhanced barrier protection, as evidenced by a high contact angle of 105.8°, while maintaining a moderate average surface temperature of 60.2 °C, and a minimal exposure time of 20 s during the SiO_x nanocoating deposition process. This processing temperature is well below those typically required for conventional coating techniques, such as hot-melt and fluidized pan coating, which often operate at average temperatures in the range 75−100 °C.

3.2. Surface Characterization of SiO_x Nanocoating

The surface morphological characteristics of pristine and optimized plasma-assisted SiO_x-nanocoated tablets were examined using SEM. Overall clear and distinct morphological differences were evident between the pristine and SiO_x-nanocoated tablet surfaces across progressively higher magnifications. In particular, the pristine tablet exhibited a compact and relatively homogeneous surface, characterized by smooth, tightly packed particle domains and minimal surface asperities, which are indicative of the mechanical compression process used during tablet formation[53] (Figure 4a). In contrast, the SiO_x-nanocoated tablets displayed a uniformly distributed granular surface morphology, consistent with the formation of a continuous nanoscale coating under the optimized plasma deposition conditions (Figure 4b). This homogeneous SiO_x layer remained clearly discernible at higher magnifications, confirming the effectiveness of the CAP-assisted process in generating a uniform, conformal nanoscale coating without compromising the integrity of the underlying formulation at either the micro- or macroscale.

To further validate the homogeneous distribution of the SiO_x nanocoating, elemental surface mapping for carbon, oxygen, titanium, and silicon was performed on pristine and SiO_x-nanocoated tablets. Titanium was included in the elemental analysis as it is inherently present in the tablet from a commercially applied polymeric film coating introduced during manufacturing. As expected, the pristine tablets showed clear signals for carbon, oxygen, and titanium, with no detectable silicon on the surface (Figure 4c). In contrast, the application of the optimized SiO_x nanocoating resulted in a pronounced and uniformly distributed silicon signal across the tablet surface (Figure 4d). This uniform silicon distribution confirms the effectiveness of the plasma-assisted process in achieving consistent and conformal SiO_x coverage without localized aggregation or surface defects. Additionally, a marginal reduction in the relative signals of carbon, oxygen, and titanium was observed, consistent with surface coverage by the deposited SiO_x layer. To further quantify the change in the elemental composition between the pristine and SiO_x-nanocoated tablets, the obtained EDS spectra were deconvoluted to extract the relative atomic percentages of carbon, oxygen, titanium, and silicon (Figure 4e,f). As observed, the SiO_x-nanocoated tablet exhibited a 6.8% reduction in the carbon content and a 12.2% reduction in titanium, along with a 2.5% increase in oxygen and a 4.5% increase in silicon relative to the pristine tablet (Figure 4g). To further characterize the functional groups on the surface of the SiO_x-nanocoated tablets, FTIR analysis was performed. As shown in Supporting Information Figure S4, the nanocoating exhibits distinct peaks at 1177 cm^{-1}, 804 cm^{-1}, and 475 cm^{-1}, corresponding to Si−O−Si stretching, bending, and rocking bands respectively, which are key characteristics of SiO_x networks.[54] These compositional shifts, supported by elemental mapping and chemical bond characterization, collectively confirm the successful deposition and uniform integration of the SiO_x nanocoating onto the tablet surface. The coating thickness was measured to be 403.551 ± 52.188 nm (Supporting Information Figure S5), further validating the optimized plasma-assisted process parameters.

3.3. Mechanical Integrity and Dissolution Characterization

To assess the mechanical stability of the SiO_x nanocoating on the tablet, friability was measured for both the pristine and the SiO_x-nanocoated tablets. As observed in Supporting Information, Figure S6, both the pristine and SiO_x-nanocoated tablets showed no significant change in the visual appearance before and after friability testing. Additionally, to quantitatively assess coating integrity, tablet mass was measured before and after friability testing for both the pristine and SiO_x-nanocoated tablets to determine the percentage weight loss. As observed, the overall weight loss of the SiO_x-nanocoated tablets was 0.07%, comparable to that of the pristine samples (0.12%), and both values were well below 1%, which is within the acceptable limit for coated pharmaceutical products as specified by USP

https://doi.org/10.1021/acsanm.6c00822
ACS Appl. Nano Mater. 2026, 9, 8294−8310

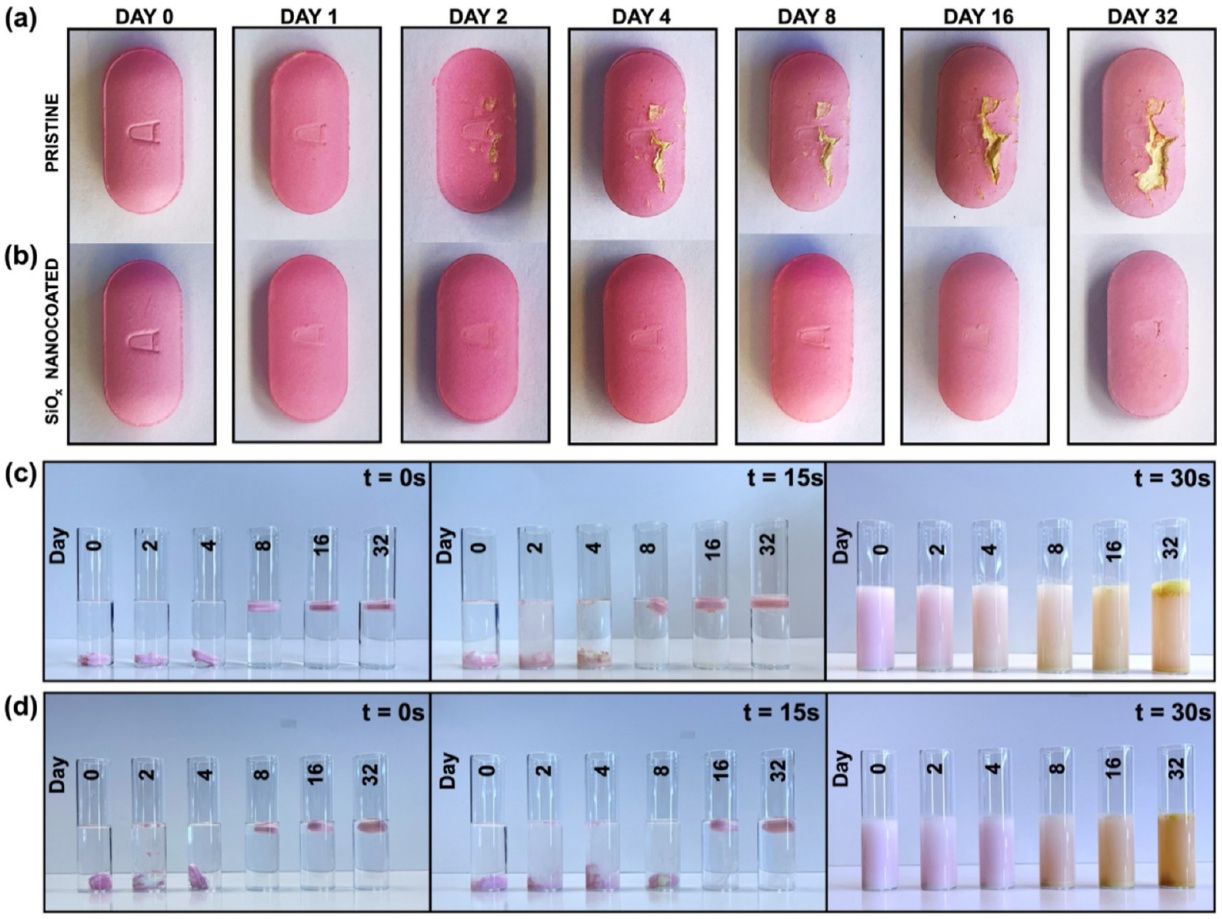

Figure 5. Visual dissolution characterization of pristine and optimized CAP-assisted SiO_x-nanocoated AMOX tablets exposed to accelerated aging conditions (40 °C, 75% RH). (a) Photographic images of pristine tablets and (b) SiO_x-nanocoated tablets subjected to accelerated aging conditions retrieved at 0, 2, 4, 8, 16, and 32 days. (c) Rapid disintegration screening images of pristine tablets retrieved from each time point, captured at 0, 15, and 30 s after immersion, and (d) corresponding dissolution images of SiO_x-nanocoated tablets at the same time intervals.

<1216> guidelines.[47] Furthermore, no flaking, chipping, or visually apparent surface damage was observed on the SiO_x-nanocoated tablets at either the macroscopic or microscopic level. These results clearly elucidate the mechanical robustness, adhesion, and durability of the SiO_x nanocoating under handling and transport conditions.

Additionally, to investigate changes in tablet disintegration and dissolution behavior induced by SiO_x nanocoating, time-dependent UV−vis absorption analysis was performed on dissolution media collected at defined time points. As shown in Supporting Information Figure S7a, the spectra exhibited characteristic absorbance peaks at 228 and 272 nm corresponding to the β-lactam and carbonyl chromophores of AMOX, which increased monotonically in intensity over time for the pristine tablets, consistent with progressive drug dissolution.[55] Similarly, the SiO_x-nanocoated tablets displayed comparable peak positions and temporal intensity evolution, indicating no apparent alteration in disintegration or diffusion behavior (Supporting Information Figure S7b). To further quantitatively compare the dissolution profiles, the absorbance intensities at 228 and 272 nm were tracked over time (Supporting Information Figure S7c). As observed, both pristine and SiO_x-nanocoated tablets exhibited similar absorbance profiles from 5 to 60 min with negligible differences in final intensity. Collectively, the preserved friability and unchanged dissolution response confirm that the SiO_x nanocoating maintains both the mechanical integrity and the intrinsic dissolution characteristics of the tablet formulation under physiological buffer conditions.

3.4. Accelerated Stability Test and Characterization

To assess the stability of the optimized plasma-assisted SiO_x nanocoating and its effectiveness in preventing moisture ingress and mitigating hydrolytic/thermal degradation of the API formulation, an accelerated aging study was performed under elevated temperature and humidity conditions. For this test, the pristine and SiO_x-nanocoated tablets were subjected to accelerated aging conditions and tested at predetermined time points (0, 2, 4, 8, 16, and 32), enabling direct comparison. Photographic images of the tablets, captured at various time points throughout the study, are presented in Figure 5a. As observed, the pristine tablets exhibited visible surface cracking, reaching 0.73% as early as 24 h under accelerated aging conditions, with the extent of damage progressively worsening over time. By day 32, these tablets demonstrated significant softening, surface peeling, pronounced discoloration, and 14.22% overall surface damage, indicating moisture ingress into the tablet excipients. This behavior could be attributed to the absorption of moisture by the excipients, particularly the disintegrants, which swell and exert internal pressure causing the TiO_2-based polymeric film coating to crack.[27] In contrast, the SiO_x-nanocoated tablets remained largely intact throughout the 32 day study period. Surface cracking was not observed

https://doi.org/10.1021/acsanm.6c00822
ACS Appl. Nano Mater. 2026, 9, 8294−8310

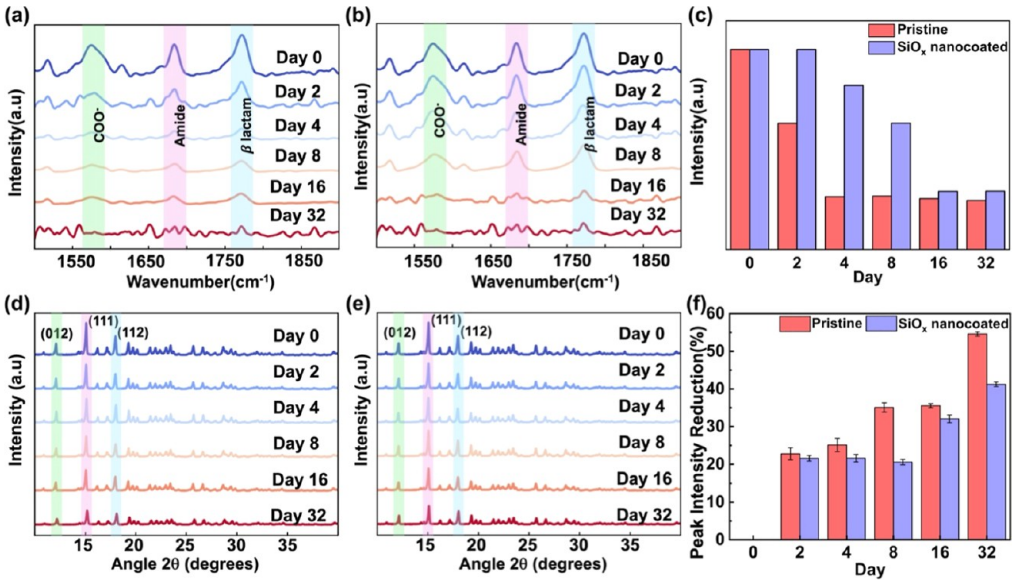

Figure 6. Chemical and structural characterization of pristine and CAP-assisted SiO_x-nanocoated AMOX tablets subjected to accelerated aging (40 °C, 75% RH) over 32 days. FTIR spectra of characteristic AMOX functional groups (carboxylate, amide, and β-lactam ring), retrieved at 0, 2, 4, 8, 16, and 32 days for (a) pristine and (b) SiO_x-nanocoated tablets, with (c) corresponding changes in the β-lactam ring intensity. PXRD patterns of (d) pristine and (e) SiO_x-nanocoated tablets over the same time course, and (f) summary of the reduction in diffraction peak intensity for the three major characteristic peaks of AMOX, relative to the pristine day 0 sample.

until day 16, and only minimal discoloration was noted by day 32, with overall surface damage reaching 2.73%, indicating that the SiO_x nanocoating effectively mitigated moisture ingress and maintained the tablet's structural integrity (Figure 5b). To further substantiate the observed visual change in the stability conditions, the rapid disintegration behavior of the tablets was assessed at each time point by monitoring the tablets at 0, 15, and 30 s (Figure 5c). Overall, the pristine tablets upon progressive aging showed delayed and inconsistent immediate disintegration and wetting, with the tablets floating in the medium. Such failure in disintegrant characteristics can promote hydrolytic degradation of amoxicillin as moisture exposure facilitates cleavage of the β-lactam ring, ultimately diminishing its antimicrobial activity.[56] In contrast, SiO_x-nanocoated tablets showed rapid immediate disintegration profiles through day 8, with minimal discoloration and no floating observed (Figure 5d). These results suggest that the SiO_x nanocoating provides protection against moisture-induced changes, helping to preserve rapid dispersion, surface appearance, and color under elevated temperature and humidity for up to 8 days without significantly affecting the function of disintegrants and other excipients.

To further assess changes in the chemical stability of the API in the formulation under accelerated aging, FTIR analysis was performed on both pristine and SiO_x-nanocoated tablets collected at different time points. As shown in Figure 6a, the API in pristine tablets at day 0 exhibited clear characteristic signatures of AMOX, including the β-lactam carbonyl (C═O) stretch at 1769 cm^{-1}, the amide C═O stretch at 1688 cm^{-1}, and the asymmetric stretch of the carboxylate (COO^-) group at 1587 cm-1.[56,57] However, under accelerated humidity and temperature conditions, a significant reduction in the characteristic vibrational bands was observed, with notable changes occurring within 2 days, as shown in Figure 6a. Possible degradation of AMOX under these conditions primarily results from hydrolysis of the β-lactam ring, leading to a measurable decrease particularly in the intensity of the 1769 cm^{-1} peak. These vibrational peaks continued to deteriorate in samples retrieved from days 4 to 16, with irregular and inconsistent spectral features appearing by day 32. In contrast, the API in SiO_x-nanocoated tablets exhibited significantly enhanced chemical stability, with no noticeable reduction in the β-lactam peak intensity until day 8 of exposure as shown in Figure 6b. However, after 16 days of incubation, a considerable decrease was observed, which continued to decline through day 32. To further quantify the reduction in the β-lactam peak, the peak intensities are summarized in Figure 6c. As observed, the API from pristine tablets showed a 33% reduction by day 2, increasing to 66% and 83% by days 8 and 32, respectively. This sharp decrease aligns with the hydrolytic ring opening, suggesting a potential loss of antibiotic potency. In contrast, the API in SiO_x-nanocoated tablets demonstrated significantly enhanced chemical stability, with no noticeable reduction in β-lactam peak intensity until day 2. Upon further incubation under accelerated aging conditions, a 17% decrease was observed by day 4, followed by a 38% decline by day 8, and continued to gradually decrease until day 32, indicating the retention of chemical integrity of the API in SiO_x-nanocoated tablets.

To assess changes in the crystalline structure of the API in the tablets upon exposure to accelerated aging conditions, PXRD analysis was performed on pristine and SiO_x-nanocoated tablets retrieved at different time points. As observed in Figure 6d,e, both the API from pristine and SiO_x-nanocoated tablets exhibited clear diffraction peaks at 12.14°, 15.10°, 17.17°, 18.04°, and 16.22°, corresponding to the (021), (111), (112), (023), and (102) planes of AMOX, respectively.[58] Notably, in the pristine samples, although the characteristic peaks remained identifiable, the peak intensity gradually decreased over time, suggesting a progressive loss of long-range crystalline order, likely due to environmental exposure and moisture ingress (Figure 6d). On the other hand, the API from SiO_x-nanocoated tablets maintained consistent diffraction peak intensities across all major diffraction planes through day

https://doi.org/10.1021/acsanm.6c00822
ACS Appl. Nano Mater. 2026, 9, 8294−8310

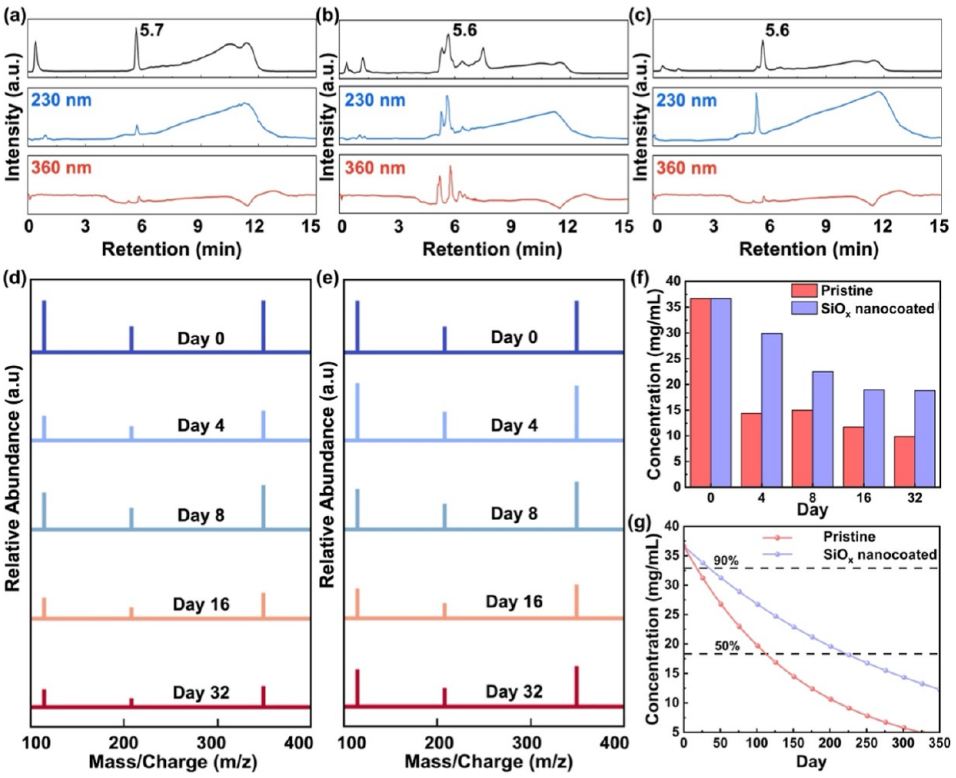

Figure 7. Chemical characterization of individual species associated with AMOX in pristine and CAP-assisted SiO_x-nanocoated tablets subjected to accelerated aging (40 °C, 75% RH). HPLC retention time chromatograms with UV−Vis detection at 230 and 360 nm for (a) AMOX Standard, and AMOX in (b) pristine and (c) SiO_x-nanocoated tablets upon exposure to 8 days of accelerated aging. LC/MS characteristic spectra of AMOX in (d) pristine and (e) SiO_x-nanocoated tablets retrieved at 0, 4, 8, 16, and 32 days during accelerated aging. (f) Quantified AMOX concentration at each time point in the accelerated aging study, calculated against the standard calibration curve. (g) Theoretical projection of AMOX concentration over 350 days under ambient conditions (25 °C, 40% RH) based on first-order degradation kinetics.

8, with no significant reduction observed, as shown in Figure 6e. Beyond day 8, a gradual decrease in peak intensity was observed, indicating the onset of minor alterations in the crystal structure, though the overall long-range order remained better preserved than that in the pristine counterparts under identical aging conditions. To further quantify the observed changes in peak intensities, the average peak intensity reduction relative to the day 0 pristine tablet was determined from the three major diffraction peaks, providing a measure of alterations in the crystalline domain dimensions under accelerated aging conditions. As shown in Figure 6f, the API from pristine tablets exhibited an initial decrease in average peak intensity of 22.77% by day 2, reaching 35.08% by day 8, followed by a sharp decline to ∼54.58% by day 32, indicating progressive crystalline breakdown over time. In contrast, the SiO_x-nanocoated API tablets maintained a relatively consistent ∼21% reduction in peak intensity until day 8, gradually increasing to 41.24% by day 32, indicating enhanced crystal structure stability under accelerated aging conditions. These results clearly demonstrate that the optimized SiO_x-nanocoated tablets preserve the chemical integrity and crystalline structure of the API for up to 8 days under accelerated aging conditions.

3.5. Drug Concentration Analysis

To identify changes in the chemical features of the pristine and SiO_x-nanocoated tablets subjected to accelerated aging, UV−vis spectroscopy was performed on dissolution solutions to track variations in characteristic absorbance features. As observed, API from pristine tablets at day 0 exhibited distinct absorbance maxima at 228 and 272 nm, corresponding to the β-lactam ring and carbonyl functional groups of AMOX, respectively[59] (Supporting Information Figure S8a). With progressive aging, a gradual reduction in β-lactam peak intensity was observed, accompanied by the emergence of a broad absorbance at 358 nm, attributed to phenol hydroxypyrazine (ADP6), a known AMOX degradant.[60,61] The intensity of this degradant-associated peak increased approximately 4-fold between days 2 and 8, followed by a further 2-fold rise by day 16, and continued increasing by day 32, as summarized in Supporting Information Figure S8b. This spectral evolution reflects a progressive loss of native AMOX absorbance features, concurrent with the growth of ADP6-related bands, consistent with the conjugated double-bond structure shown schematically in Supporting Information Figure S8c. In contrast, the API in the SiO_x-nanocoated tablets retained the β-lactam and carbonyl peaks with minimal change until day 8, with no detectable ADP6 signal during this period (Supporting Information Figure S8d). However, the β-lactam peak intensity decreased, while a new absorbance band at 358 nm emerged and progressively increased through day 32 (Supporting Information Figure S8e). These results indicate that the SiO_x nanocoating limits the moisture-driven chemical degradation of the API in the tablet under accelerated aging conditions, supporting the trends observed in the FTIR and XRD analyses discussed previously.

To validate the identified spectral changes from UV−vis and resolve the individual chemical species associated with AMOX degradation under accelerated aging, HPLC-UV analysis was

https://doi.org/10.1021/acsanm.6c00822
ACS Appl. Nano Mater. 2026, 9, 8294−8310

performed. For this test, dissolution solutions from pristine and SiO_x-nanocoated tablets collected at day 8 of accelerated aging were analyzed, along with a standard amoxicillin (AMOX-d_4) as the reference. As observed, the chromatograms were recorded at two characteristic wavelengths, 230 and 360 nm, corresponding respectively to the β-lactam absorption band of amoxicillin and the absorbance region associated with its major degradation product, ADP6.[60] Particularly, the AMOX-d_4 standard showed a dominant retention peak at approximately 5.7 min, corresponding to the intact AMOX parent compound (Figure 7a). The corresponding UV trace at 230 nm showed a sharp, well-defined peak at the same retention time, confirming strong β-lactam absorption, whereas the 360 nm trace remained featureless, consistent with the absence of chromophoric degradants in pure AMOX-d_4. On the other hand, the pristine tablet subjected to accelerated aging for 8 days showed a markedly different chromatographic profile compared with AMOX-d_4, as shown in Figure 7b. The primary retention peak was broader and less defined with additional peaks appearing between 5 and 7 min and at longer retention times. These changes were observed in both the 230 and 360 nm traces and indicate partial degradation of the β-lactam structure, with a new absorbance peak near 360 nm, consistent with the formation of conjugated degradation products under humid conditions. In contrast, the SiO_x-nanocoated tablet retrieved at the same aging period exhibited a chromatographic profile nearly identical to that of AMOX-d_4, as shown in Figure 7c. The major retention peak was observed at approximately 5.6 min with comparable intensity and sharpness, and the 360 nm trace remained featureless throughout the run. The absence of secondary peaks and chromophoric bands confirms that the SiO_x nanocoating effectively prevented the chemical degradation of the β-lactam moiety and maintained the structural integrity of the API during accelerated exposure.

To assess the extent of API concentration retention in SiO_x-nanocoated tablets compared to pristine controls under accelerated aging conditions, a quantitative LC/MS-based assay was performed. All API in pristine and SiO_x-nanocoated tablets exhibited a characteristic chromatographic retention time of 5.7 to 5.8 min, consistent with the AMOX-d_4 internal standard (shown in Supporting Information Figure S9). To further characterize the molecular composition and verify the structural integrity after chromatographic separation, mass spectrometry was performed on all pristine and SiO_x-nanocoated tablet samples. As shown in Figure 7d,e, all API in tablets retrieved at various time points exhibited four consistent characteristic peaks, confirming the reproducibility of the fragmentation pattern. In particular, the ion at m/z 353 corresponded to the protonated AMOX molecule, reflecting the near-complete mass after the loss of one water molecule, while the peak at m/z 114 was attributed to fragmentation of the thiazolidine ring. Additionally, the ion at m/z 212 resulted from cleavage between the β-lactam ring and side chain, producing p-hydroxyphenyl glycine, and a less prominent peak at m/z 366 represented intact AMOX, likely arising from the protonated parent ion in the sample.[56] However, a pronounced reduction in the intensity of all characteristic peaks was observed for the API in pristine tablets recovered from later time points, indicating a decline in the detectable AMOX ions in the sample during progressive degradation under accelerated aging conditions (Figure 7d). In contrast, the API in SiO_x-nanocoated tablets maintained consistent peak intensity with minimal reduction observed until day 8, confirming enhanced chemical stability under identical conditions, as shown in Figure 7e.

To further quantify the observed peak intensity changes, the AMOX concentration in the medium was calculated from the corresponding standard calibration curve and is summarized in Figure 7f. As observed, both the pristine and SiO_x-nanocoated tablet exhibited an initial API concentration of approximately 36 mg·mL^{-1}, validating that the plasma deposition process did not significantly alter the initial concentration of the formulation. On the other hand, during progressive incubation at elevated temperature and humidity, the API in pristine tablets showed a marked reduction in the antibiotic concentration to 14.36, 14.90, 11.76, and 9.84 mg·mL^{-1} on days 4, 8, 16, and 32, respectively. In contrast, the SiO_x-nanocoated tablets retained higher concentrations, measuring 29.89 mg·mL^{-1} on day 4, followed by 22.47 mg·mL^{-1}, 18.95 mg·mL^{-1}, and 18.76 mg·mL^{-1} on days 8, 16, and 32. These results demonstrate significant retention of the initial API concentration in the SiO_x-nanocoated tablets, with substantially higher levels even after 8 days of accelerated aging.

To project the long-term performance of the SiO_x-nanocoated tablets, the measured effective concentration under elevated conditions was used to estimate the available concentration when stored under ambient conditions of 25 °C and 40% RH (as described in Supporting Information Note 1). These calculations predict the amount of intact AMOX that may remain accessible under standard storage conditions, offering insight into the expected retention of the effective concentration over time. The reaction rate constants were derived from the measured concentrations assuming first-order kinetics.[62] These constants were applied to the humidity corrected Arrhenius equation to estimate the decline in available concentration and predict concentration profiles at room temperature (as described in the Supporting Information Equations S1−S3).[62,63] The extrapolated data to 350 days, presented in Figure 7g, showed a 90% decline to the initial concentration within 17 days and a 50% concentration reduction at 112 days for the API in pristine tablets. In contrast, the SiO_x-nanocoated tablet demonstrated markedly enhanced stability, maintaining 90% of its initial API concentration for 37 days and delaying the 50% reduction point to 224 days. This approximate 2-fold extension in shelf life conferred by the SiO_x nanocoating confirms its effectiveness in preserving the chemical and structural integrity of the API in tablets under projected ambient conditions.

To demonstrate the generalizability of the SiO_x nanocoating strategy beyond the AMOX formulation, accelerated aging combined with UV−vis stability analysis was conducted on penicillin V and aspirin as chemically distinct model APIs. For penicillin V, both pristine and SiO_x-nanocoated tablets were exposed to 40 °C and 75% RH for 8 days, and UV−vis absorption spectra were collected over time to monitor chemical changes. As observed in Supporting Information Figure S10a, in the pristine tablets, two characteristic absorption peaks were observed at ∼220 nm and ∼270 nm, corresponding to the β-lactam and carbonyl groups, respectively.[64] After 8 days of accelerated aging, an absorption band at ∼350 nm was observed and attributed to the formation of penicillanic acid (PA), a known degradation product of penicillin V.[65] In contrast, the SiO_x-nanocoated tablets retained the β-lactam and carbonyl peaks without additional bands, confirming that the SiO_x nanocoating effectively

https://doi.org/10.1021/acsanm.6c00822
ACS Appl. Nano Mater. 2026, 9, 8294−8310

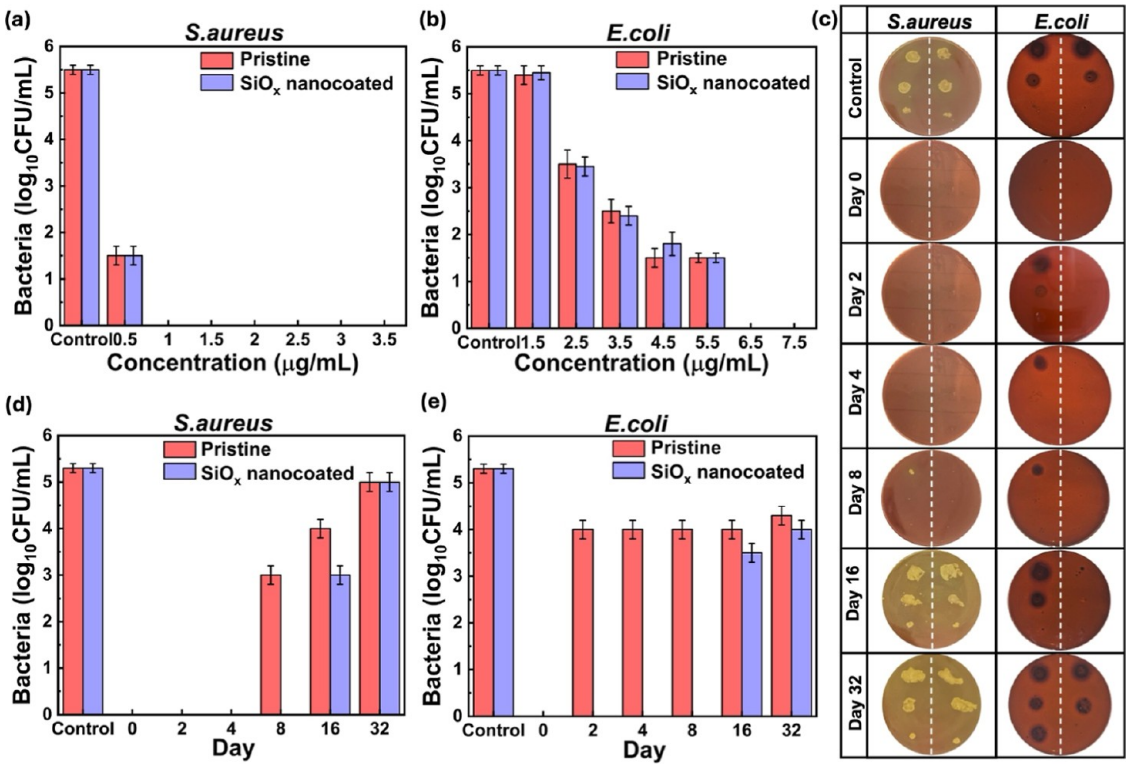

Figure 8. Antibacterial efficacy of AMOX in pristine and CAP-assisted SiO_x-nanocoated tablets. MIC analysis of AMOX in pristine and as-prepared SiO_x-nanocoated tablets against (a) *S. aureus* and (b) *E. coli*. (c) Representative plate images of antibacterial efficacy of AMOX against *S. aureus* and *E. coli* for pristine and CAP-assisted SiO_x-nanocoated tablets subjected to accelerated aging (40 °C, 75% RH) conditions at MIC. Quantitative assessment of antibacterial efficacy over the aging period for (d) *S. aureus* and (e) *E. coli*. (*Staphylococcus aureus*: *S. aureus*, *Escherichia coli*: *E. coli*).

preserved the molecular structure and prevented degradation under these conditions (Supporting Information Figure S10b).

Similarly, aspirin, a common nonsteroidal anti-inflammatory drug used to treat pain, fever, and inflammation, was subjected to the same accelerated stability conditions for 32 days.[66] The as-procured aspirin tablets exhibited a characteristic absorption peak at ∼ 230 nm, which corresponds to the parent aspirin molecule, as shown in Supporting Information Figure S10c.[67] After stability exposure, an additional absorption band emerged near 300 nm, indicating the formation of salicylic acid through hydrolytic degradation.[66] In comparison, the SiO_x-nanocoated aspirin tablets retained the original absorption profile with no detectable peak near 300 nm, demonstrating complete suppression of the degradation pathway (Supporting Information Figure S10c).[67] These findings collectively validate the broader applicability of CAP-assisted SiO_x nanocoating as a protective barrier that maintains chemical stability in diverse moisture-sensitive pharmaceutical formulations.

3.6. Antibacterial Activity

To assess changes in bactericidal potency under accelerated aging conditions, an in vitro antibacterial analysis was performed. The antibacterial activity of the released antibiotic against a 10^5 CFU·mL^{-1} suspension of *S. aureus* and *E. coli* was evaluated using a minimum inhibitory concentration (MIC) assay. Both pristine and SiO_x-nanocoated tablets were dissolved in designated media, and the resulting solutions were serially diluted to obtain API concentrations ranging from 0 to 10 μg·mL^{-1} in 0.5 μg·mL^{-1} increments. These dilutions were then introduced into the bacterial suspensions for assessment. As shown in Figure 8a, the control groups for *S. aureus* exhibited no significant change in bacterial population without antibiotic API exposure. In contrast, at 0.5 μg·mL^{-1}, a 10^5 CFU·mL^{-1} reduction was observed, and at higher concentrations, bacterial populations were reduced to undetectable levels, indicating complete bacterial elimination. On the other hand, no significant reduction in the *E. coli* bacterial population was observed until 1.5 μg·mL^{-1}, after which a progressive reduction was observed (Figure 8b). A complete 10^5 CFU·mL^{-1} reduction at the bacterial population was observed in concentrations above 5.5 μg·mL^{-1}. The difference in the response between *S. aureus* and *E. coli* is attributed to differences in their cell wall structures. *S. aureus*, with a thick, multilayer peptidoglycan cell wall, is more susceptible to lower concentrations of AMOX, which targets the synthesis of this structure (as shown in Supporting Information Figure S11a).[68,69] In contrast, *E. coli* has an additional outer membrane that acts as a barrier, limiting the permeability of AMOX and requiring higher concentrations to achieve comparable inhibition of bacterial growth (Supporting Information Figure S11b).[68,69] These results clearly indicate that the SiO_x-nanocoated tablets show no significant change in antibacterial potency compared to that of the pristine tablets. Additionally, based on these findings, 1 μg·mL^{-1} and 6.5 μg·mL^{-1} were identified as the MICs for *S. aureus* and *E. coli*, respectively, and were therefore used for the accelerated stability analysis.

To further assess changes in the potency of the API in the tablets under accelerated aging conditions, antibacterial tests were conducted on both pristine and SiO_x-nanocoated tablets collected at different time points. As shown in Figure 8c, the pristine tablets exhibited a clear reduction in antibacterial

https://doi.org/10.1021/acsanm.6c00822
ACS Appl. Nano Mater. 2026, 9, 8294−8310

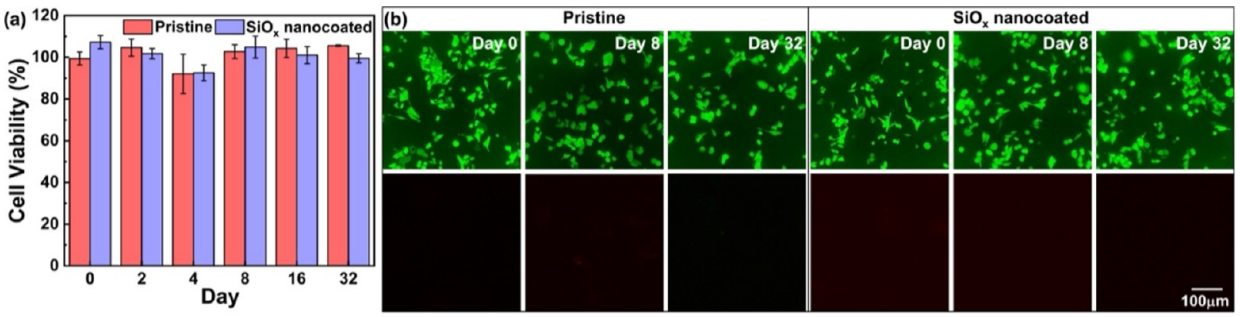

Figure 9. Biocompatibility characteristics of pristine and CAP-assisted SiO_x nanocoated tablets under accelerated aging conditions (40 °C, 75% RH). (a) MTT cell viability assay of HCT-8 cells after exposure to pristine and SiO_x-nanocoated tablets retrieved at various time points normalized against the control. (b) Live−dead fluorescence staining images of pristine and SiO_x-nanocoated tablets retrieved on days 0, 8, and 32.

potency against *S. aureus* by day 8 and against *E. coli* by day 2. In contrast, the SiO_x-nanocoated tablets retained antibacterial activity against both *S. aureus* and *E. coli* through day 8, indicating that the plasma-deposited SiO_x nanocoating effectively preserved the API's antimicrobial efficacy during accelerated aging. To quantify this observation, the individual CFUs from the selective plates were enumerated for each bacterial population and are represented in Figure. 8d,e. As shown in Figure 8d, the *S. aureus* bacterial population exposed to 0.5 $\mu g \cdot mL^{-1}$ of antibiotic exhibited a consistent $\sim 10^5$ CFU·mL^{-1} reduction after 4 days of accelerated testing. However, a drastic reduction in antibacterial potency was observed with the pristine tablets after 8 days of incubation under controlled stress conditions. In contrast, the SiO_x-nanocoated tablets retained antibacterial properties up to day 8, after which a significant decline was observed. On the other hand, with the *E. coli*, a drastic loss of the antibacterial potency was observed with the pristine antibiotic within 2 days of incubation under high temperature and humidity conditions (Figure 8e). However, as expected, the SiO_x-nanocoated tablet exhibited a marked preservation of antibacterial activity observing a complete 10^5 CFU·mL^{-1} reduction for up to 8 days, after which a significant decline in potency was observed. These results further substantiate the effectiveness of the SiO_x nanocoating in preserving the antimicrobial efficacy of API in tablets for up to 8 days under accelerated aging conditions.

3.7. Biocompatibility Analysis

Finally, to validate the biocompatibility characteristics of the SiO_x-nanocoated tablets and its sustained cytocompatibility under accelerated aging conditions, an in vitro assay was performed using physiologically relevant human gut epithelial HCT-8 cells. Initially, the change in metabolic activity of mammalian cells upon exposure to the SiO_x-nanocoated tablets was assessed using a standard MTT assay with pristine tablets collected at various time points serving as controls. In this assay, the tetrazolium MTT salt is reduced by mitochondrial dehydrogenases in metabolically active cells, leading to the formation of insoluble purple formazan crystals.[70] The quantity of formazan is directly proportional to the percentage of cell viability of the mammalian cells exposed to the API tablets retrieved from each time point of the accelerated aging test. As shown in Figure 9a, cells exposed to both pristine and SiO_x-nanocoated tablets exhibited viability above 90%, confirming the sustained biocompatibility of the SiO_x nanocoating even after exposure to elevated temperature and humidity conditions for 32 days. On the other hand, to visualize changes in cell viability and morphology upon exposure of tablets from each time point, a live/dead staining assay was performed. In this assay, the green-fluorescent dye (calcein AM) permeates viable cells and is converted by intracellular esterases into calcein, producing intense green fluorescence, while the red-fluorescent dye (ethidium homodimer) enters only compromised cells with damaged membranes, binds to nucleic acids, and emits red fluorescence to indicate cell death.[70] As shown in Figure 9b, a high green to red fluorescence ratio was observed for the pristine tablets at various time points under accelerated aging conditions from day 0 to day 32. A similar green/red fluorescence ratio was observed for the SiO_x-nanocoated tablets, confirming the long-term cytocompatibility characteristics of the developed coating technology.

Overall, these results clearly demonstrate that the developed CAP-assisted SiO_x nanocoating technology provides an effective moisture barrier that preserves the chemical integrity, structural stability, and antimicrobial potency of thermally sensitive APIs under accelerated aging conditions. In addition to performance, the scalability of this approach is supported by both, its high processing throughput and low material consumption, as quantified under the fabrication conditions employed in this study. Precursor usage corresponds to a material cost of ∼0.6 cents per tablet, underscoring the economic feasibility of CAP-assisted deposition at scale (as described in Supporting Information Note 2). Moreover, the atmospheric-pressure operation of CAP enables compatibility with continuous roll-to-roll configurations, with areal throughputs corresponding to effective coating rates of ∼ 183 tablets per minute for tablet-scale geometries, indicating suitability for manufacturing-relevant production volumes.[43,44] By enabling direct, low-thermal-load deposition and maintaining compatibility with pharmaceutical substrates, this approach holds promise for broader application to other moisture-sensitive drug products and for seamless integration into existing manufacturing processes. Prior to widespread adoption by the pharmaceutical industry, this technology should be further evaluated through USP-regulated stability testing in physiologically relevant media and extended to in vivo animal studies to comprehensively assess its translational potential and industrial applicability. Given the introduction of a plasma-based coating process, regulatory translation will require a demonstration that critical quality attributes such as dissolution, bioavailability, and stability remain unchanged under cGMP-compliant manufacturing conditions. In parallel, process-level validation, including control of plasma parameters, coating uniformity, batch-to-batch reproducibility, assessment of residual species and potential leachables, and

https://doi.org/10.1021/acsanm.6c00822
ACS Appl. Nano Mater. 2026, 9, 8294−8310

subsequent clinical evaluation under FDA regulatory guidance, supports practical industrial implementation. With the enhanced stability performance demonstrated in this study and the potential to extend tablet shelf life, this technology may offer meaningful economic and humanitarian benefits by improving drug durability and global accessibility of vulnerable drug products, reducing waste, and increasing access to pharmaceutical products in resource-limited areas around the world.

4. CONCLUSIONS

This work demonstrates the use of CAP-assisted scalable manufacturing technology to deposit SiO_x nanocoatings onto oral pharmaceutical formulations, providing an effective barrier that enhances stability and protects against moisture and thermal degradation. Systematic optimization of the plasma scan speed and nozzle-to-substrate distance was performed to achieve uniform SiO_x nanocoating formation, ensuring effective humidity-barrier protection without compromising the integrity of the API in the formulation. Results revealed that the optimized CAP-assisted SiO_x nanocoating retained over 50% of the initial API's chemical integrity and antibiotic concentration for 16 days, maintained antimicrobial efficacy for 8 days, and sustained cytocompatibility under accelerated aging conditions, compared with rapid degradation and potency loss in pristine counterparts. Collectively, these findings validate the potential of the developed plasma-assisted nanocoating approach to extend the shelf life and stability of moisture-sensitive drugs under demanding storage and distribution environments. Moreover, the demonstrated process scalability and compatibility with existing pharmaceutical formats position this technology as a promising platform for advancing tablet coating strategies toward routine industrial application.

■ ASSOCIATED CONTENT

Supporting Information

The Supporting Information is available free of charge at https://pubs.acs.org/doi/10.1021/acsanm.6c00822.

Additional results and supporting figures, including schematic illustration of antibacterial assay and biocompatibility assay, surface wettability characterization, surface FTIR characterization, cross section microscopy of surface nanocoating, tablet friability analysis, UV−vis absorption drug release kinetics profiles, UV−vis absorption drug stability analysis, AMOX HPLC chromatogram, additional UV−vis absorption drug stability analysis of penicillin V and aspirin, schematic representation of AMOX interaction with bacteria well walls, equations for theoretical prediction of drug degradation kinetics using humidity corrected Arrhenius Equation, and additional note on scalability of the CAP deposition technique (PDF)

■ AUTHOR INFORMATION

Corresponding Author

Rahim Rahimi − *Electrical and Computer Engineering, Purdue University, West Lafayette, Indiana 47907, United States; Birck Nanotechnology Research Center, Bindley Bioscience Center, School of Materials Engineering, and Weldon School of Biomedical Engineering, Purdue University, West Lafayette, Indiana 47907, United States;* orcid.org/0000-0001-5302-782X; Email: rrahimi@purdue.edu

Authors

Advika Vidhyadhiraja − *Electrical and Computer Engineering, Purdue University, West Lafayette, Indiana 47907, United States; Birck Nanotechnology Research Center and Bindley Bioscience Center, Purdue University, West Lafayette, Indiana 47907, United States;* orcid.org/0009-0003-8078-7877

Akshay Krishnakumar − *Electrical and Computer Engineering, Purdue University, West Lafayette, Indiana 47907, United States; Birck Nanotechnology Research Center and Bindley Bioscience Center, Purdue University, West Lafayette, Indiana 47907, United States;* orcid.org/0000-0002-0626-3843

Devendra Sarnaik − *Birck Nanotechnology Research Center, Bindley Bioscience Center, and School of Materials Engineering, Purdue University, West Lafayette, Indiana 47907, United States*

Zhongxia Shang − *Birck Nanotechnology Research Center, Purdue University, West Lafayette, Indiana 47907, United States;* orcid.org/0000-0002-2974-2599

Kinam Park − *Departments of Biomedical Engineering and Pharmaceutics and Weldon School of Biomedical Engineering, Purdue University, West Lafayette, Indiana 47907, United States;* orcid.org/0000-0001-8202-6084

Complete contact information is available at: https://pubs.acs.org/10.1021/acsanm.6c00822

Notes

The authors declare no competing financial interest.

■ ACKNOWLEDGMENTS

The authors would like to acknowledge the support staff and engineers of School of Electrical and Computer Engineering, School of Materials Engineering, Birck Nanotechnology Center, and Bindley Bioscience Center at Purdue University. The authors would like to thank Lynne S. Taylor and Emily G. Benson for expert guidance in refining the experimental interpretation and terminology used throughout the manuscript. We would like to also thank Yu Han-Hallet and the Metabolomics Profiling Facility for assisting in the liquid chromatography/mass spectroscopic analysis.

■ REFERENCES

(1) Vargason, A. M.; Anselmo, A. C.; Mitragotri, S. The Evolution of Commercial Drug Delivery Technologies. *Nat. Biomed. Eng.* **2021**, *5* (9), 951−967.

(2) Subbiah, V. The next Generation of Evidence-Based Medicine. *Nat. Med.* **2023**, *29* (1), 49−58.

(3) Grand View Research. Pharmaceutical Market Size & Share, Industry Report, 2030; San Francisco https://www.grandviewresearch.com/industry-analysis/pharmaceutical-market-report (accessed 2025−05−21).

(4) Kim, J.; De Jesus, O. *Medication Routes of Administration*; StatPearls Publishing LLC.: Treasure Island (FL), 2023.

(5) Dolan, S. A.; Arias, K. M.; Felizardo, G.; Barnes, S.; Kraska, S.; Patrick, M.; Bumsted, A. APIC Position Paper: Safe Injection, Infusion, and Medication Vial Practices in Health Care. *Am. J. Infect. Control* **2016**, *44* (7), 750−757.

(6) Williams, S. R.; Nix, D. A.; Patel, K. H. Drug Storage and Stability. In *Wilderness Medicine*; Elsevier, 2007; pp 2251−2260.

(7) Cyriac, J. M.; James, E. Switch over from Intravenous to Oral Therapy: A Concise Overview. *J. Pharmacol. Pharmacother.* **2014**, *5* (2), 83−87.
(8) Alqahtani, M. S.; Kazi, M.; Alsenaidy, M. A.; Ahmad, M. Z. Advances in Oral Drug Delivery. *Front. Pharmacol.* **2021**, *12*, 618411.
(9) González-González, O.; Ramirez, I. O.; Ramirez, B. I.; O'Connell, P.; Ballesteros, M. P.; Torrado, J. J.; Serrano, D. R. Drug Stability: ICH versus Accelerated Predictive Stability Studies. *Pharmaceutics* **2022**, *14* (11), 2324.
(10) Hotha, K. K.; Roychowdhury, S.; Subramanian, V. Drug-Excipient Interactions: Case Studies and Overview of Drug Degradation Pathways. *Am. J. Analyt. Chem.* **2016**, *07* (01), 107−140.
(11) Hemingway, R.; Baertschi, S. W.; Benstead, D.; Campbell, J. M.; Coombs, M.; Huang, Z.; Khalaf, R.; Ott, M. A.; Ponting, D. J.; Reid, D. L.; Stevenson, N. G.; Webb, S. J.; White, A.; Zelesky, T. In Silico Prediction of Pharmaceutical Degradation Pathways: A Benchmarking Study Using the Software Program Zeneth. *Org. Process Res. Dev.* **2024**, *28* (3), 674−692.
(12) de Lemos, M. L.; Mathers, B.; Badry, N.; Hamata, L.; Lo, K. Challenges of Dispensing Costly Tablets with Short Shelf-Life. *J. Oncol. Pharm. Pract.* **2019**, *25* (1), 210−213.
(13) Lizarraga, E.; Zabaleta, C.; Palop, J. A. Thermal Stability and Decomposition of Pharmaceutical Compounds. *J. Therm. Anal. Calorim.* **2007**, *89* (3), 783−792.
(14) Allinson, J. G.; Dansereau, R. J.; Sakr, A. The Effects of Packaging on the Stability of a Moisture Sensitive Compound. *Int. J. Pharm.* **2001**, *221* (1−2), 49−56.
(15) Waterman, K. C.; Macdonald, B. C. Package Selection for Moisture Protection for Solid, Oral Drug Products. *J. Pharm. Sci.* **2010**, *99* (11), 4437−4452.
(16) Shukla, S.; Halli, P.; Khalid, M. K.; Lundström, M. Waste Pharmaceutical Blister Packages as a Source of Secondary Aluminum. *JOM* **2022**, *74* (2), 612−621.
(17) Veronica, N.; Liew, C. V.; Heng, P. W. S. Insights on the Role of Excipients and Tablet Matrix Porosity on Aspirin Stability. *Int. J. Pharm.* **2020**, *580*, 119218.
(18) Khan, M. H.; Hatanaka, K.; Sovannarith, T.; Nivanna, N.; Casas, L. C. C.; Yoshida, N.; Tsuboi, H.; Tanimoto, T.; Kimura, K. Effects of Packaging and Storage Conditions on the Quality of Amoxicillin-Clavulanic Acid − an Analysis of Cambodian Samples. *BMC Pharmacol. Toxicol.* **2013**, *14* (1), 33.
(19) Kiron, S. S.; Shirwaikar, A.; Saritha, M.; Rajagopal, P. L.; Sreejith, K. R. Influence of Storage Condition on the Shelf Life of Amoxicillin Tablets. *Elixir Pharmacy* **2013**, *64*, 19146−19150.
(20) Akhtar Nehal Ahmed, S.; Ravindra Patil, S.; Sadique Khan, M. K.; Shaban Khan, M. Tablet Coating Techniques: Concept and Recent Trends. *Int. J. Pharm. Sci. Rev. Res.* **2021**, *66* (1), 43−53.
(21) Nguyen, H. T.; Van Duong, T.; Taylor, L. S. Enteric Coating of Tablets Containing an Amorphous Solid Dispersion of an Enteric Polymer and a Weakly Basic Drug: A Strategy to Enhance in Vitro Release. *Int. J. Pharm.* **2023**, *642*, 123139.
(22) Seo, K.-S.; Bajracharya, R.; Lee, S. H.; Han, H.-K. Pharmaceutical Application of Tablet Film Coating. *Pharmaceutics* **2020**, *12* (9), 853.
(23) Thoma, K.; Bechtold, K. Influence of Aqueous Coatings on the Stability of Enteric Coated Pellets and Tablets. *Eur. J. Pharm. Biopharm.* **1999**, *47* (1), 39−50.
(24) Mandal, R. K.; Saini, P.; Pal, R.; Pandey, P.; Dubey, A. Coating Tablets, Compositions, Recent Advancement and Current Status: A Comprehensive Review. *J. Drug Delivery Ther.* **2024**, *14* (10), 182−195.
(25) Christian, P.; Ehmann, H. M. A.; Coclite, A. M.; Werzer, O. Polymer Encapsulation of an Amorphous Pharmaceutical by Initiated Chemical Vapor Deposition for Enhanced Stability. *ACS Appl. Mater. Interfaces* **2016**, *8* (33), 21177−21184.
(26) Rashidi, T.; Shakeri, A. Effects of Nano Zinc Oxide and Nano Chitosan on the Taste Masking Paracetamol Granules. *Drug Dev. Ind. Pharm.* **2024**, *50* (6), 495−510.
(27) Moseson, D. E.; Benson, E. G.; Cao, Z.; Bhalla, S.; Wang, F.; Wang, M.; Zheng, K.; Narwankar, P. K.; Simpson, G. J.; Taylor, L. S. Impact of Aluminum Oxide Nanocoating on Drug Release from Amorphous Solid Dispersion Particles. *Mol. Pharmaceutics* **2023**, *20* (1), 593−605.
(28) Zhang, Y.; Xiong, G. M.; Ali, Y.; Boehm, B. O.; Huang, Y. Y.; Venkatraman, S. Layer-by-Layer Coated Nanoliposomes for Oral Delivery of Insulin. *Nanoscale* **2021**, *13* (2), 776−789.
(29) Narayan, R. J.; Monteiro-Riviere, N. A.; Brigmon, R. L.; Pellin, M. J.; Elam, J. W. Atomic Layer Deposition of TiO2 Thin Films on Nanoporous Alumina Templates: Medical Applications. *JOM* **2009**, *61* (6), 12−16.
(30) Van Duong, T.; Nguyen, H. T.; Wang, F.; Wang, M.; Narwankar, P. K.; Taylor, L. S. Surface Nanocoating of High Drug-Loading Spray-Dried Amorphous Solid Dispersions by Atomic Layer Coating: Excellent Physical Stability under Accelerated Storage Conditions for Two Years. *Int. J. Pharm.* **2022**, *620*, 121747.
(31) Haghshenas-Lari, M. J.; Mostoufi, N.; Sotudeh-Gharebagh, R. Medicinal Stability of Vitamin C Coated with TiO2 by ALD. *Part. Sci. Technol.* **2018**, *36* (6), 727−733.
(32) Hautala, J.; Kääriäinen, T.; Hoppu, P.; Kemell, M.; Heinämäki, J.; Cameron, D.; George, S.; Juppo, A. M. Atomic Layer Deposition−A Novel Method for the Ultrathin Coating of Minitablets. *Int. J. Pharm.* **2017**, *531* (1), 47−58.
(33) Petlin, D. G.; Tverdokhlebov, S. I.; Anissimov, Y. G. Plasma Treatment as an Efficient Tool for Controlled Drug Release from Polymeric Materials: A Review. *J. Controlled Release* **2017**, *266*, 57−74.
(34) Susut, C.; Timmons, R. B. Plasma Enhanced Chemical Vapor Depositions to Encapsulate Crystals in Thin Polymeric Films: A New Approach to Controlling Drug Release Rates. *Int. J. Pharm.* **2005**, *288* (2), 253−261.
(35) Dufour, T. From Basics to Frontiers: A Comprehensive Review of Plasma-Modified and Plasma-Synthesized Polymer Films. *Polymers* **2023**, *15* (17), 3607.
(36) Benson, E. G.; Moseson, D. E.; Bhalla, S.; Wang, F.; Wang, M.; Zheng, K.; Narwankar, P. K.; Taylor, L. S. Dissolution of Copovidone-Based Amorphous Solid Dispersions: Influence of Atomic Layer Coating, Hydration Kinetics, and Formulation. *J. Pharm. Sci.* **2025**, *114* (1), 323−335.
(37) Schütze, A.; Jeong, J. Y.; Babayan, S. E.; Park, J.; Selwyn, G. S.; Hicks, R. F. The Atmospheric-Pressure Plasma Jet: A Review and Comparison to Other Plasma Sources. *IEEE Trans. Plasma Sci.* **1998**, *26*, 1685−1694.
(38) Heredia-Rivera, U.; Krishnakumar, A.; Kasi, V.; Rana, M. M.; Gopalakrishnan, S.; Nejati, S.; Gundala, G.; Barnard, J. P.; Wang, H.; Rahimi, R. Cold Atmospheric Plasma Deposition of Antibacterial Polypyrrole−Silver Nanocomposites on Wearable Electronics for Prolonged Performance. *J. Mater. Chem. C Mater.* **2024**, *12* (31), 11861−11876.
(39) Rahman, M. M.; Krishnakumar, A.; Vidhyadhiraja, A.; Xu, K.; Rana, M. M.; Alcaraz, A. M.; Zhang, X.; Rahimi, R. Cold Atmospheric Plasma-Assisted Corrosion-Resistant SiOx Coating on Temporary Orthopedic Fixation Implants. *Mater. Chem. Phys.* **2026**, *348*, 131672.
(40) Rahman, M. M.; Krishnakumar, A.; Vidhyadhiraja, A.; Rana, M. M.; Sarnaik, D.; Aguirre-Cruz, G.; Stanciu, L.; Rahimi, R. Cold Atmospheric Plasma−Assisted Deposition of SiOx−Ag Nanocomposites for SERS-Based Detection of Listeria Monocytogenes in Complex Food Matrices. *Sens. Actuators B Chem.* **2026**, *457*, 139663.
(41) Kasi, V.; Rahman, M. M.; Tien, J.-H.; Rana, M. M.; Vidhyadhiraja, A.; Sarnaik, D.; Rivera, U. H.; Bahr, D.; Rahimi, R. Improved Corrosion Protection of Copper in Electronic Devices via CAP-Assisted Multilayer SiOx Coatings. *Appl. Mater. Today* **2024**, *41*, 102517.
(42) Kasi, V.; Mahabubur Rahman, M.; Krishnakumar, A.; Rivera, U. H.; Sarnaik, D.; Sinha, M.; Rahimi, R. Cold Atmospheric Plasma-Assisted Deposition of Ammonium Functionalized Glass Coating for Enhanced Antibacterial Properties. *J. Mater. Chem. C Mater.* **2025**, *13*, 16252−16264.

https://doi.org/10.1021/acsanm.6c00822
ACS Appl. Nano Mater. 2026, 9, 8294−8310

(43) Elam, F. M.; Starostin, S. A.; Meshkova, A. S.; van der Velden-Schuermans, B. C. A. M.; Bouwstra, J. B.; van de Sanden, M. C. M.; de Vries, H. W. Atmospheric Pressure Roll-to-roll Plasma Enhanced CVD of High Quality Silica-like Bilayer Encapsulation Films. *Plasma Processes Polym.* **2017**, *14* (7), 1600143.
(44) Kusano, Y.; Bredgaard, K.; Pan, H.; Bardenstein, A. L. Roll-to-Roll SiOx Synthesis on Polyethylene Terephthalate Film by Atmospheric-Pressure Plasma-Assisted Chemical Vapor Deposition. *Materials* **2024**, *17* (19), 4694.
(45) Gao, Y.; Zhang, Y.; Hong, Y.; Wu, F.; Shen, L.; Wang, Y.; Lin, X. Multifunctional Role of Silica in Pharmaceutical Formulations. *AAPS PharmSciTech* **2022**, *23*, 90.
(46) Sarnaik, D.; Krishnakumar, A.; Nejati, S.; Sullivan, C. R.; Cross, T.-W. L.; Campbell, W. W.; Johnson, J. S.; Rahimi, R. A. Smart Capsule with a Bacteria- and PH-Triggered Enteric Polymer Coating for Targeted Colonic Microbiome Sampling. *Acta Biomater.* **2025**, *199*, 412−427.
(47) Osei-Yeboah, F.; Sun, C. C. Validation and Applications of an Expedited Tablet Friability Method. *Int. J. Pharm.* **2015**, *484* (1−2), 146−155.
(48) United States Pharmacopeial Convention. ⟨1216⟩ Tablet Friability. In *United States Pharmacopeia and National Formulary (USP 47−NF 42)*; United States Pharmacopeial Convention: Rockville, MD, **2024**.
(49) Thompson, P.; Cox, D. E.; Hastings, J. B. Rietveld Refinement of Debye−Scherrer Synchrotron X-Ray Data from Al2O3. *J. Appl. Crystallogr.* **1987**, *20* (2), 79−83.
(50) Kasi, V.; Tien, J. H.; Rahman, M. M.; Rana, M. M.; Heredia Rivera, U. A.; Shang, Z.; Vidhyadhiraja, A.; Zhang, J.; Youngblood, J. P.; Bahr, D. F.; Rahimi, R. Enhanced Corrosion Protection of Printed Circuit Board Electronics Using Cold Atmospheric Plasma-Assisted SiOx Coatings. *ACS Appl. Mater. Interfaces* **2024**, *16* (36), 48293−48306.
(51) Alencar, L. C. B.; Santana, C. P.; Silva, K. M. A.; Nóbrega, F. P.; Correia, L. P.; Santos, W. M.; Andrade, F. H. D.; Santos, F. S.; Macêdo, R. O.; Medeiros, A. C. D. Thermal Study of Active Pharmaceutical Ingredients Used as Analgesics by DTA and DSC Coupled to Photovisual System. *Chem. Thermodyn. Therm. Anal.* **2022**, *7*, 100072.
(52) Zelesky, T.; Baertschi, S. W.; Foti, C.; Allain, L. R.; Hostyn, S.; Franca, J. R.; Li, Y.; Marden, S.; Mohan, S.; Ultramari, M.; Huang, Z.; Adams, N.; Campbell, J. M.; Jansen, P. J.; Kotoni, D.; Laue, C. Pharmaceutical Forced Degradation (Stress Testing) Endpoints: A Scientific Rationale and Industry Perspective. *J. Pharm. Sci.* **2023**, *112* (12), 2948−2964.
(53) Dailymed. Amoxicillin−DailyMed. U.S. National Library of Medicine. https://dailymed.nlm.nih.gov/dailymed/lookup.cfm?setid=bb7733f8-6aad-4273-84a0-ef472630203f (accessed 2025−05−14).
(54) Carneiro, J. O.; Machado, F.; Rebouta, L.; Vasilevskiy, M. I.; Lanceros-Méndez, S.; Teixeira, V.; Costa, M. F.; Samantilleke, A. P. Compositional Optical and Electrical Characteristics of SiOx Thin Films Deposited by Reactive Pulsed DC Magnetron Sputtering. *Coatings* **2019**, *9* (8), 468−469.
(55) Ataklti, A.; Alemu, K.; Abebe, B. Study of the Self-Association of Amoxicillin, Thiamine and the Hetero-Association with Biologically Active Compound Chlorgenic Acid. *Afr. J. Pharm. Pharmacol.* **2016**, *10* (18), 393−402.
(56) Ecke, A.; Westphalen, T.; Retzmann, A.; Schneider, R. J. Factors Affecting the Hydrolysis of the Antibiotic Amoxicillin in the Aquatic Environment. *Chemosphere* **2023**, *311*, 136921.
(57) Nugrahani, I.; Soewandhi, S. N.; Ibrahim, S. Solid State Interaction between Amoxicillin Trihydrate and Potassium Clavulanate. *Malays. J. Pharm. Sci.* **2007**, *5* (1), 45−75.
(58) Narkar, M.; Sher, P.; Pawar, A. Stomach-Specific Controlled Release Gellan Beads of Acid-Soluble Drug Prepared by Ionotropic Gelation Method. *AAPS PharmSciTech* **2010**, *11* (1), 267−277.
(59) Palma, E.; Ellison, L.; Meza, E.; Griko, Y. Calorimetric Evaluation of Amoxicillin Stability in Aqueous Solutions. *Mathews Journal of Pharmaceutical Science* **2016**, *2* (1), 008.
(60) Gozlan, I.; Rotstein, A.; Avisar, D. Amoxicillin-Degradation Products Formed under Controlled Environmental Conditions: Identification and Determination in the Aquatic Environment. *Chemosphere* **2013**, *91* (7), 985−992.
(61) Salois, A.; Perez, I.; Palma, E.; Goolish, E.; Griko, Y. Evaluation of the Chemical Integrity of Beta-Lactam Antibiotics by Iodine-Based Assay. *J. Biosci. Med.* **2015**, *03* (11), 91−99.
(62) Kuzman, D.; Bunc, M.; Ravnik, M.; Reiter, F.; Žagar, L.; Bončina, M. Long-Term Stability Predictions of Therapeutic Monoclonal Antibodies in Solution Using Arrhenius-Based Kinetics. *Sci. Rep.* **2021**, *11* (1), 20534.
(63) Naveršnik, K.; Jurečič, R. Humidity-Corrected Arrhenius Equation: The Reference Condition Approach. *Int. J. Pharm.* **2016**, *500* (1−2), 360−365.
(64) Derakhshani, E.; Naghizadeh, A.; Mortazavi-Derazkola, S. Phyto-Assisted Synthesis of Magnetic NiFe2O4 Nanocomposite Using the Pulicaria Gnaphalodes Methanolic Extract for the Efficient Removal of an Antibiotic from the Aqueous Solution: A Study of Equilibrium, Kinetics, Isotherms, and Thermodynamics. *AQUA—Water Infrastructure, Ecosystems and Society* **2023**, *72* (11), 2035−2051.
(65) Escamilla, P.; Bartella, L.; Sanz-Navarro, S.; Percoco, R. M.; Di Donna, L.; Prejanò, M.; Marino, T.; Ferrando-Soria, J.; Armentano, D.; Leyva-Pérez, A.; Pardo, E. Degradation of Penicillinic Antibiotics and B-Lactamase Enzymatic Catalysis in a Biomimetic Zn-Based Metal−Organic Framework. *Chem.—Eur. J.* **2023**, *29* (51), No. e202301325.
(66) Sherikar, O.; Mehta, P. Comprehensive Assessment of Degradation Behavior of Aspirin and Atorvastatin Singly and in Combination by Using a Validated RP-HPLC Method. *Sci. Pharm.* **2013**, *81* (1), 195−210.
(67) Damle, M. C.; Sinha, P. K.; Bothara, K. G. A validated stability indicating HPTLC method for determination of aspirin and clopidogrel bisulphate in combined dosage form. *Eurasian J. Anal. Chem.* **2009**, *4*, 152−160.
(68) Akhavan, B. J.; Khanna, N. R.; Vijhani, P. *Amoxicillin*; StatPearls Publishing LLC., 2025.
(69) Ding, X.; Su, J.; Chen, X.; Zhang, S.; Li, M.; yang, J.; Wang, Z.; Wang, J.; Wang, W.; Sun, D.; Wang, G. Application of Synergistic β-Lactamase Inhibitors and Antibiotics in the Treatment of Wounds Infected by Superbugs. *Arabian J. Chem.* **2022**, *15* (7), 103936.
(70) Krishnakumar, A.; Gallina, N. L. F.; Sarnaik, D.; McCain, R. R.; Crain, C.; Tipton, M.; Seleem, M.; Bhunia, A. K.; Rahimi, R. Microneedles for Enhanced Bacterial Pathogen Inactivation and Accelerated Wound Healing. *Adv. Mater. Technol.* **2024**, *9* (16), 2400219.

https://doi.org/10.1021/acsanm.6c00822
ACS Appl. Nano Mater. 2026, 9, 8294−8310